Neutral Atmospheres

I. C. F. Mueller-Wodarg, D. F. Strobel, J. I. Moses, J. H. Waite, J. Crovisier, R. V. Yelle, S. W. Bougher, R. G. Roble

Abstract This paper summarizes the understanding of aeronomy of neutral atmospheres in the solar system, discussing most planets as well as Saturn's moon Titan and comets. The thermal structure and energy balance is compared, highlighting the principal reasons for discrepancies amongst the atmospheres, a combination of atmospheric composition, heliocentric distance and other external energy sources not common to all. The composition of atmospheres is discussed in terms of vertical structure, chemistry and evolution. The final section compares dynamics in the up-

I. C. F. Mueller-Wodarg
Blackett Laboratory, Imperial College, Prince Consort Road, London SW7 2BW, U.K., e-mail: i.mueller-wodarg@imperial.ac.uk

D. F. Strobel
Johns Hopkins University, 3400 North Charles Street, Baltimore, MD 21218, USA, e-mail: strobel@jhu.edu

J. I. Moses
Lunar and Planetary Institute, 3600 Bay Area Boulevard, Houston TX 77058, USA, e-mail: moses@lpi.usra.edu

J. H. Waite
Southwest Research Institute, 6220 Culebra, San Antonio, TX 78228, USA, e-mail: hwaite@swri.edu

J. Crovisier
LESIA, Observatoire de Paris, 92195 Meudon, France, e-mail: Jacques.Crovisier@obspm.fr

R. V. Yelle
Lunar and Planetary Laboratory, University of Arizona, Tucson, AZ 85721, USA, e-mail: yelle@lpl.arizona.edu

S. W. Bougher
Department of Atmospheric, Oceanic and Space Sciences, College of Engineering, University of Michigan, 2455 Hayward Street, Ann Arbor, MI 48109, USA, e-mail: bougher@umich.edu

R. G. Roble
High Altitude Observatory, National Center for Atmospheric Research, P.O. Box 3000, Boulder, Colorado 80307, USA, e-mail: roble@hao.ucar.edu

per atmospheres of most planets and highlights the importance of vertical dynamical coupling as well as magnetospheric forcing in auroral regions, where present. It is shown that a first order understanding of neutral atmospheres has emerged over the past decades, thanks to the combined effects of spacecraft and Earth-based observations as well as advances in theoretical modeling capabilities. Key gaps in our understanding are highlighted which ultimately call for a more comprehensive programme of observation and laboratory measurements

1 Introduction

All planets, many moons and some of the smaller objects in the solar system are surrounded by gas envelopes which may in the widest definition be referred to as atmospheres. However, important distinctions can be made between these atmospheres. The first important distinction is that between permanent and transient atmospheres; the former are atmospheres bound gravitationally by the solid body, giving them long lifetimes on the scale of the age of the solid body. Permanent atmospheres can be formed either from accretion of primordial material or outgassing processes and volcanism. Planets Venus, Earth, Mars, Pluto and all Gas Giants including moons Titan and Triton host atmospheres that are referred to as permanent. In contrast, transient atmospheres are those not sufficiently bound gravitationally, where constituents escape the gravitational field of the solid body. In these cases the presence of an atmosphere relies upon an active gas source, such as outgassing from the interior, volcanism or sputtering processes. Typical examples of transient atmospheres are comets, Jupiter's moon Io and most other moons in the solar system, planet Mercury and larger asteroids.

In this chapter permanent atmospheres of planets and moons as well as transient atmospheres of comets are discussed. The focus will remain on neutral gases only, which form the principal mass and volume of most atmospheres. Small fractions of the neutral atmosphere are ionized by solar radiation or charged particle impact processes, forming ionospheres. These may affect neutral gas properties as well via dynamical or chemical or energetic coupling, and some of the principal ion-neutral coupling processes are also reviewed in this chapter.

Table 1 compares main properties of permanent atmospheres in the solar system, such as heliocentric distance, rotation period of the solid body, principal gas composition and exospheric temperatures. It is evident from this overview that one can in terms of composition classify the atmospheres into mainly three classes, those dominated by N_2 (Earth, Titan, Triton, Pluto), CO_2 (Venus, Mars) and Hydrogen/Helium (Jupiter, Saturn, Uranus, Neptune). Of the terrestrial planets, Venus has the most substantial atmosphere with a surface pressure of around 90 bars and temperature of 733 K. Differences between the terrestrial planet atmospheres are considerable, despite their relative proximity in the solar system, while in the outer solar system most planets are Gas Giants with essentially similar atmospheres. The temperature reached asymptotically in the thermosphere, or exosphere temperature (see also sec-

tion 2), should to a first approximation be largely influenced by solar EUV radiation which is absorbed in that region of the atmosphere, and yet Table 1 shows no consistent trend of these temperatures with distance from the Sun. Venus, the planet closest to the Sun, has the lowest exosphere temperature of all planets, while the Gas Giants Jupiter and Saturn have exospheric temperatures larger than those of Mars, Venus and often Earth, despite their much larger distances from the Sun. Understanding these first order differences between atmospheres in the solar system will be one of the aims of this chapter. Comparative studies between different planets give us a deep understanding of the main physics in planetary atmospheres since applying the same basic physics to different boundary conditions (distance from Sun, mass of solid body, composition) produces very different worlds. The paper will discuss the thermal structures (Section 2), composition and chemistry (Section 3) as well as dynamics (Section 4) and highlight open questions to be addressed by future studies (Section 5). Although discussions concentrate on our solar system, many of the basic physics are believed to apply similarly to extrasolar planets and understanding our own solar system forms the basis for understanding other solar systems.

2 Thermal structure and energy balance

2.1 Planets and moons

The thermal structure of a planetary atmosphere is normally described with nomenclature originally introduced to describe the globally averaged temperature profile of the Earth's atmosphere, using as principal criterion the vertical thermal gradient. The Earth's lower atmosphere is known as the troposphere (see Fig. 1). It is characterized by a relatively constant negative temperature gradient, $\sim$-6.5 K km^{-1}. This lapse rate is determined both by an intermediate value of the moist adiabatic lapse rate (which can be as low as -3 K km^{-1} up to the dry adiabat of -9.8 K km^{-1}) and the large scale dynamics of the troposphere. At the equator the top of the troposphere, known as the tropopause is approximately 17 km above the surface with a temperature of $\sim$190 K and it slopes downward towards the poles to an altitude of only $\sim$8 km but with a higher temperature $\sim$210-230 K, depending on season. By comparison the surface temperature varies from 300 K at the equator to 250 K at the poles.

Photochemistry of molecular oxygen leads to the formation of ozone, whose photochemistry driven by absorption of solar ultraviolet radiation results in atmospheric heating and the formation of the stratosphere, which has a positive temperature gradient of $\sim$2 K km^{-1}. The upper boundary of the stratosphere (called the stratopause) is at 50 km and the 1 mbar level, where the temperature reaches a relative maximum of $\sim$290 K at the summer pole and $\sim$250 K at the winter pole with a global average of $\sim$270 K. Above the stratosphere is the region known as the mesosphere, which is characterized by a negative temperature gradient of $\sim$-3 K km^{-1}, as a consequence

of the ozone heating rate decreasing more rapidly with altitude than the CO_2 infrared cooling rate and consistent with the observed ratio of ozone density to CO_2 density declining with height. Collectively, the stratosphere and mesosphere are known as the middle atmosphere.

The upper boundary of the mesosphere is known as the mesopause and is typically at 85-90 km and approximately the 1 μbar level. The globally averaged mesopause temperature is $\sim$185 K, but over the summer pole it drops to $\sim$130 K and can be a high as 220 K over the winter pole due to a large scale meridional circulation, which transports heat to the winter pole with adiabatic cooling over the summer pole and adiabatic heating over the winter pole. Calculations have shown that the thermal structure and dynamics of the mesosphere cannot be reproduced when assuming a radiative equilibrium case (Geller, 1983) and a wave drag term is needed. Physically, this represents the momentum deposited by dissipating or breaking gravity waves, tides and planetary waves in the atmosphere, and for simplicity it is often approximated by a linear Rayleigh friction term (Schoeberl and Strobel, 1978). More comprehensive models use gravity wave parameterization schemes to simulate the momentum deposition, as described further in Section 4. Note that this

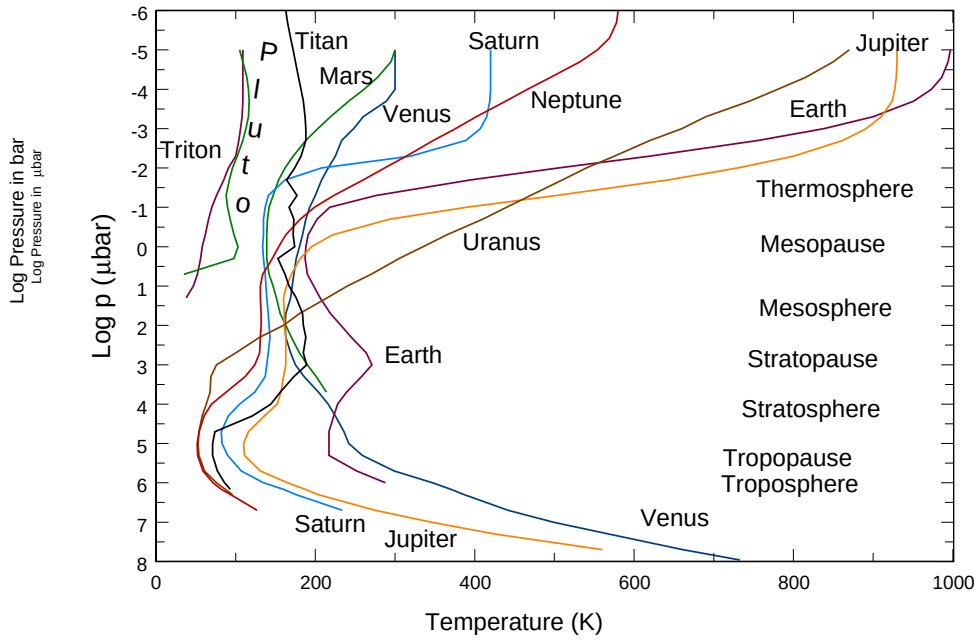

Fig. 1 Temperatures versus pressure for Venus, Earth, Mars, Jupiter, Saturn, Titan, Uranus, Neptune, Triton and Pluto.

affects both the dynamics and the thermal structure via advection of energy and adiabatic heating and cooling.

The region above the mesopause is the thermosphere which is characterized by a very rapid temperature increase of $\sim$10-20 K km^{-1} and asymptotically attains a constant (isothermal) temperature at high altitudes, commonly called the exospheric temperature and denoted by T_∞. This temperature can be as low as 600 K during solar minimum activity and as high as 2000 K during solar maximum conditions. In addition, there is a diurnal variation in exospheric temperature of $\sim$30%, which has a phase-shifted maximum from the subsolar point and minimum from the antisolar point of $\sim$2-3 hr caused by thermospheric winds. The basic physics of the thermosphere is intense heating by absorption of short wavelength solar ultraviolet radiation ($<$170 nm) in the dissociation and/or ionization of molecules and atoms and the downward transport of thermal energy by heat conduction due to the absence of infrared active molecules, such as CO_2, capable of radiating thermal energy away locally. The mesopause is the region where radiative cooling of downward conducted energy becomes most effective, giving it the lowest temperature. The mesopause can therefore essentially be regarded as the heat sink for the thermosphere. Thermospheric heating is supplemented by auroral energy deposition in the polar regions (primarily Joule heating and partly particle precipitation heating) which may exceed solar heating rates.

Even though the heating and cooling processes in the atmospheres of other planets and satellites may have a different relative balance, vertical temperature profiles on all planets show similar features (Fig. 1) and this nomenclature originally used for the Earth's atmosphere is adopted for their atmospheres and temperature profiles as well. The Earth's twin planet Venus has a massive CO_2 atmosphere with a surface temperature of 733 K at low latitudes and slightly warmer (737 K) at higher latitudes with essentially constant surface pressure of 92.1 bar (Table 1). It has a very extended troposphere with a lapse rate of -8.98 K km^{-1} up to about 35 km and 6 bar, which is close to the adiabatic lapse rate, but stable. Above 35 km where haze layers are present on Venus, the temperature notably departs from this lapse rate, indicating heating and this trend continues into the cloud region between 50-70 km (1-0.03 bar), with one exception of a convective layer within the clouds at $\sim$55 km (0.5 bar). At 58 km, where the pressure is 0.3 bar and temperature is $\sim$270 K, the atmosphere becomes substantially more stable in analogy with the Earth's atmosphere, this level is denoted as the tropopause and the region above as the stratosphere, even though the temperature continues to decrease up to 95 km to $\sim$162-167 K and pressure $\sim$0.1 mbar. On the dayside the temperature ramps up to an asymptotic value of $\sim$230-325 K (the range from solar minimum to solar maximum activity), whereas on the nightside it decreases to $\sim$100 K. Given the slow rotation of Venus, the dayside-nightside temperature contrast is a subsolar bulge to antisolar hole. On the dayside the region between 95-160 km is known as the dayside thermosphere, whereas on the nightside in effect the stratosphere extends up to the exobase at 160 km, where the pressure is $\sim$20 pbar, but the "nightside thermosphere" is called the cryosphere. The dayside model atmosphere in Fig. 1 is based on measurements by the Pioneer Venus atmospheric probes (Seiff, 1983).

The other terrestrial CO_2 atmosphere is the thin atmosphere of Mars with surface pressure of 6 mbar and temperature $\sim$214 K, but which varies from 140-270 K. On Mars the troposphere extends to about 50 km and 10 μbar, where occasionally CO_2-ice clouds are present and the temperature is $\sim$145 K. Above this level, as for Venus, the change in atmospheric stability justifies calling this region the stratosphere and the temperature gradually decreases to about 140 K depending on latitude at 100 km and 40 nbar. This level is the mesopause, as the temperature increases rapidly above it to an asymptotic value of 180 K during low solar activity to as high as 325 K during solar maximum and when Mars is closest to the Sun. With an eccentricity of 0.093, the solar flux varies by 45% over the orbit.

The key to understanding the differences in exospheric temperatures on Venus and Mars appears to lie in the role of radiative cooling. As shown by Bougher et al. (1994), 15 μm emissions from CO_2 largely originate from vibrationally excited CO_2 and cause significant cooling in regions of non-local thermodynamics equilibrium (LTE). Collisions of O atoms with CO_2 molecules cause the main vibrational excitation of CO_2 and hence enhance this radiative cooling process, implying that larger values of O/CO_2 ratios favor radiative cooling. Typical values for Venus are $O/CO_2 \approx$ 7-16%, while on Mars they have, in the absence of direct O measurements (see 5.6), been calculated to lie between 2-4%. Despite the uncertainty of this ratio on Mars due to the lack of direct O measurements there, the values indicate a significantly lower ratio on Mars than Venus, making CO_2 15 μm cooling more effective on Venus than Mars. This finding is supported by the relatively weak temperature changes with solar activity on Venus compared with Mars and also Earth (Forbes et al., 2006). On Venus, CO_2 cooling acts as thermostat to solar energy deposition. At higher solar activity levels, dissociation of O_2 and CO_2 becomes more effective, and hence the abundances of O, leading to more effective vibrational excitation of CO_2 and ultimately more effective cooling, offsetting much of the temperature change which would result from the larger solar flux. Theoretical calculations of the cooling rate rely on knowledge of the CO_2-O relaxation rate, which to-date is poorly constrained, with values from laboratory measurements ranging from 1.2 ± 0.2 to $6\pm3\times10^{-12}$ cm^3s^{-1} (Pollock et al., 1993; Sharma and Wintersteiner, 1990; Shved et al., 1991; Castle et al., 2006), as discussed also by Huestis et al. (2008).

The giant planets are mostly H_2-He atmospheres with deep tropospheres that have slightly superadiabatic lapse rates consistent with the outward convection of internal heat slowly working its way out from gravitational contraction during formation and condensational heating associated with phase changes. Convection extends up to the cloud tops where the transition to radiative equilibrium occurs. The stratospheres are in radiative equilibrium with solar heating in near-IR CH_4 bands at 3.3, 2.3, 1.6 μm augmented by solar heating of haze particles in the lower stratosphere. The radio occultation experiments performed with the Voyager spacecrafts provide a comparative data set for the pressure regions from 1-6 bars to 1-0.35 mb (cf. Table 1 in Lindal, 1992). All thermospheres are substantially warmer than would be expected on the basis of solar UV and EUV heating, an issue as yet unresolved (see Section 5). The Voyager Ultraviolet Spectrometer (UVS) solar occultation data are still the primary data sets for the thermal structure of the upper atmospheres of

Saturn, Uranus, and Neptune. For the case of Saturn, the Cassini Ultraviolet Imaging Spectrograph (UVIS) is carrying out occultation measurements which will further constrain the thermal structure of Saturn's middle and upper atmosphere.

The best vertical profiles of density, pressure, and temperature for any giant planet were obtained from the Galileo Probe's descent through Jupiter's atmosphere down to $\sim$20 bar (Seiff et al., 1997). The transition from convection to radiative equilibrium occurs at approximately 0.7 bar on Jupiter (T$\approx$136 K), which is well below the tropopause temperature minimum of 110 K at 0.1 bar. Unlike the Earth's atmosphere, the tropopause on Jupiter is purely determined by radiative processes rather than the transition from tropospheric convection to radiative equilibrium in the stratosphere. The latter is heated to $\sim$160 K by near-IR solar radiation absorbed by CH_4 and is fairly isothermal up to 5 μbar. Here the thermosphere begins and the temperature ramps up to about 940 K due to an unknown heating mechanisms. Wave heating is widely suspected to be important, but the waves detected in the Galileo Probe data were not of sufficient amplitude and did not penetrate high enough to account for the observed temperature (Section 5). Significant amounts of Joule heating are expected to be deposited in the polar regions of Jupiter and the other Gas Giants. The main problem however turns out to be the meridional redistribution of this energy, which is largely inhibited by the fast rotation of the planets and hence primarily zonal flow in the atmosphere. A recent study by Majeed et al. (2005) proposed that dynamical heating induced by the low-latitude convergence of the high-latitude-driven thermospheric circulation would deposit thermal energy in the equatorial thermosphere of Jupiter via adiabatic heating rather than direct meridional energy transport by winds. In a separate study by Smith et al. (2007) the opposite was found, whereby the equatorial thermosphere is cooled as a result of energy and momentum deposition in the auroral zones due to poleward lower thermosphere winds which close the circulation cell initiated by the equatorward flow at higher altitudes and transports energy poleward. While their study was for Saturn, the situation would largely be the same for Jupiter.

For Saturn, so far there are no publications of radio or solar occultation data taken by the Cassini spacecraft to compare with the equivalent Voyager data. Thus the data in Fig. 1 are from Voyager data sets. The basic structure mimics the structure of Jupiter's atmosphere from 5 bar up to 5 μbar with a 20-30 K offset to lower temperatures. However the Saturnian thermosphere is considerably colder than Jupiter's for reasons not entirely understood. The ice giants Uranus and Neptune have comparable temperatures in their tropospheres and lower stratospheres up to 10 mbar. Above 10 mbar, Neptune's stratosphere increases much faster than on Uranus, probably associated with the higher abundance of CH_4 on Neptune, as the Voyager UVS detected the Raman-scattered Lyman-α line at 127 nm in the Uranian airglow, which places severe limits on the stratospheric CH_4 abundance (Yelle et al., 1987). The thermal structure of Neptune's thermosphere in Fig. 1 is based on unpublished analyses by the Voyager UVS team, whereas the thermal structure of the Uranian thermosphere is based on the analysis of Stevens et al. (1993).

Titan's thermal structure has been measured most extensively by the Cassini-Huygens Mission from multiple data sets. The Voyager Mission radio and solar

occultations have now been complemented by the equivalent UVIS measurements by the Cassini spacecraft, although the data have yet to be published. The most remarkable data is from the Huygens Atmospheric Science Investigation (HASI) by the Huygens Probe which yielded the density, pressure, and temperature structure from 1270 km down to the surface (Fulchignoni et al., 2005). The remote sensing data acquired by the Cassini Composite Infrared Spectrometer (CIRS) instrument provides a global distribution of temperature over a pressure range of 10 mbar to 1 μbar. At the Probe entry latitude CIRS data is not in agreement with the Huygen ASI data as to the location and temperature of the stratopause at equatorial latitudes (Achterberg et al., 2008). Titan's stratosphere results from intense solar heating of its optically thick photochemical haze. Cooling of the upper atmosphere is dominated at high altitudes by rotational line cooling by HCN (Yelle, 1991). The topside thermosphere has a negative temperature gradient associated with adiabatic cooling from Titan's hydrodynamically expanding atmosphere (Strobel, 2008a).

The other N_2 atmospheres in the solar system with observational data are Triton and Pluto. For Triton the thermal structure has been assembled from the stellar occultation measurements reported in Elliot et al. (2000) from the surface up to about 100 km and then above from Voyager UVS solar occultation data and analysis (cf. Strobel and Summers, 1995). For Pluto, the lower atmosphere is based on stellar occultations (cf. Elliot et al. 2007) augmented at higher altitudes by theoretical modeling reported in Strobel et al. (1996) and Strobel (2008b). The higher temperatures in the lower atmosphere of Pluto are due to the thermostat capability of CH_4, whereby the near-IR 3.3 μm band absorbs solar radiation and the 7.6 μm band radiates heat away and maintains an equilibrium temperature $\sim$100 K (Yelle and Lunine, 1999). The former is augmented by heating in the 2.3 μm band and the latter by local thermal equilibrium (LTE) CO rotational line cooling. Thermal heat conduction delivers heat to the cold surface generating a steep temperature gradient for pressures greater that 2 μbar. Elliot et al. (2000) found that CH_4 heating played a non-negligible role in Triton's lower atmosphere, but the radiative equilibrium temperature is only $\sim$50 K and not as well understood as that of Pluto. At higher altitudes, solar EUV and UV heating of N_2 and CH_4, respectively, and thermal heat conduction are important for Pluto's thermosphere, whereas in Triton's thermosphere magnetospheric electron precipitation accounts for about 2/3 the total power input.

2.2 Comets

The thermodynamics of cometary atmospheres is quite different from that of the permanent atmospheres of planets due to their expansion and conversion between a collisional regime in the inner coma to a supersonic free molecular flow in the outer coma. As a result of the large size of the atmosphere compared to the nucleus, plane-parallel models cannot apply. A spherical geometry with a density proportional to $1/r^2$ (r being the distance from the centre of mass) may be adopted in a first approach.

Although the individual processes involved in the thermodynamics of the coma are well understood, their coupling with chemistry, molecular excitation and radiative trapping render their modelling difficult. Indeed, the completion of a comprehensive model including all relevant processes for a realistic description of the cometary environment is a formidable project which is far from being achieved at the present time. A recent review of this topic was given by Combi et al. (2005).

Besides rare in situ observations, information on the expansion velocity of cometary atmospheres comes from the analysis of spectral line shapes, especially of rotational lines which can be observed at high spectral resolution at radio wavelengths. Information on the temperature comes, for the collisional region of the inner coma where LTE prevails, from the simultaneous observation of several rotational lines, or from the rotational structure of vibrational or electronic bands. However, the velocities and temperatures which are retrieved by remote sensing are averaged over the instrumental field of view and along the line of sight: we do not have direct access to their profiles as a function of distance from the nucleus. Typical velocities are in the range 0.5-2.0 km s^{-1}, and temperatures in the range 10-150 K. Velocities and temperatures are both observed to increase when the heliocentric distance r_h decreases and the total gas production of the comet increases (Biver et al., 2002; Tseng et al., 2007).

Heating in a cometary atmosphere occurs from photolysis of molecules. When a molecule is photodissociated, part of the excess energy is transferred to the fragments. Heating subsequently occurs through thermalisation by collisions of the fast fragments. The process is dominated by water photolysis (Crovisier, 1989), with a heating rate of 3.3×10^{-23} W per H_2O molecule at 1 AU from the Sun. The contribution of other species is much smaller, in part because of their small abundances and partly because their photolytic rates are smaller. Heating by other exothermic chemical reactions is also negligible. Heating is effective only if the fragments can be thermalized. Water photodissociates mainly into H and OH. Because of momentum conservation, most (84%) of the translational energy is transmitted to fast hydrogen atoms. Thermalization occurs principally through collisions with water molecules, but because of the large difference in mass of H and H_2O, only a small fraction of the energy is exchanged at each collision. Many collisions are thus necessary for total thermalization (more than 20 collisions are needed for a 90% thermalization). The thermalization efficiency may be evaluated by Monte Carlo simulations.

Cooling occurs through emissions of molecular lines. Due to the low temperature of the coma, only rotational lines can be excited by collisions and contribute to cooling. Here again water plays the major role, and emissions of water rotational lines are the most efficient mechanism. Water radiative cooling can be accurately computed in the optically thin case for LTE conditions from H_2O spectroscopic data. Typical cooling rates are 10^{-23}W per H_2O molecule at 20 K, 4×10^{-22}W at 100 K. The problem is that, for high densities, optical depth effects are critical for water lines and seriously limit the efficiency of radiative cooling (the fundamental $1_{10}-1_{01}$ rotational line of water at 555 GHz is thick within 7000 km from the nucleus even for a moderately active comet with $Q[H_2O]$ =10^{28} s^{-1}). A full theoretical treatment of the problem would require knowledge of cross-sections for col-

lisions which are still largely unknown for water and self-consistent evaluation of water excitation, optical depth effects and thermodynamics of the coma atmosphere (Bockelée-Morvan and Crovisier, 1987).

Initial conditions are determined by sublimation at the nucleus surface. Exposed water ice, when freely sublimating under solar insolation at $r_h \approx 1$ AU, is expected to equilibrate at a temperature near 180 K. Indeed, analysis of the Deep Impact mission results revealed the presence of exposed water ice on the nucleus of comet 9^P/Tempel 1, but with a very small surface which can in no way explain the sublimation rate of water observed in this comet (Sunshine et al., 2006). If sublimation occurs below the nucleus surface, it is likely that the initial conditions are affected by percolation of water vapour through the surface porous mantle. The initial velocity at the surface is about 0.3 km s^{-1}, rapidly increasing to become supersonic at 0.5-0.8 km s^{-1}.

For a small comet such as 67P/Churyumov-Gerasimenko (the target of the Rosetta mission), which has a diameter of 4 km and a gas production rate of 10^{28} s^{-1} at 1 AU from the Sun, the gas density close to the nucleus surface is $\sim 7 \times 10^{11}$ cm^{-3}, and the pressure is $\sim 1.7 \times 10^{-10}$ bar. Cooling and heating are slow processes, so that close to nucleus, the coma undergoes an almost adiabatic expansion. The result is that the temperature first drops rapidly as the coma is expanding. Indeed, temperatures as low as $\sim$10 K have been observed in some cases (small comets; comets far from the Sun).

In the inner, collisional coma, purely hydrodynamical treatment of the atmosphere is possible. The thermal and velocity profiles result from the balance of the heating and cooling processes. Heating (favoured by collisions) prevails over cooling (inhibited by optical trapping) and the temperature increases with the distance to the nucleus, as shown in Figure 2. Indeed, temperatures as large as 100-150 K have been observed for comet Hale-Bopp. Outside the collisional region, the outflow regime evolves to a free molecular flow. The large transitional region - which is out of equilibrium - is difficult to model. Monte Carlo simulations are usually employed (Hodges, 1990). The size of the collisional coma depends on the gas production rate of the comet, being typically $\sim$200 km for a small comet such as 67P/Churyumov-Gerasimenko with $Q[H_2O] = 10^{28}$ s^{-1} and $\sim$200 000 km for a giant comet such as Hale-Bopp with $Q[H_2O] = 10^{31}$ s^{-1}.

Current models reproduce well, at least qualitatively, the observed expansion velocity and temperature, and their evolution with heliocentric distance and gas production rate. Comprehensive models have to consider interaction with dust and, on a larger scale, interaction with the solar wind (Ma et al., 2008).

Water sublimation is inhibited far from the Sun (at typically heliocentric distances $r_h > 4$ AU), where cometary activity is rather dominated by CO sublimation. The transition between CO-driven and H_2O-driven activity was observed in comet Hale-Bopp for which the gas production was monitored up to $r_h = 14$ AU (Biver et al., 2002). CO is the only parent molecule observed in 27P/Schwassmann-Wachmann 1 (Senay and Jewitt, 1994), a permanently active comet in a nearly circular orbit at 5.8 AU. Modelling of a CO-dominated comet is discussed by Ip (1983).

Real comets do not have spherical symmetry, as is obvious from most images of comets. This is because cometary nuclei are not spherical and not homogeneous, and because cometary activity and aeronomic processes are driven by the Sun. Axisymmetric, or even 3-D models, are needed. The modelling of the interface between the nucleus and the coma is complex, as it involves the nucleus topography, its rotation and thermal inertia, as well as its long-term thermal history (Crifo et al., 2005).

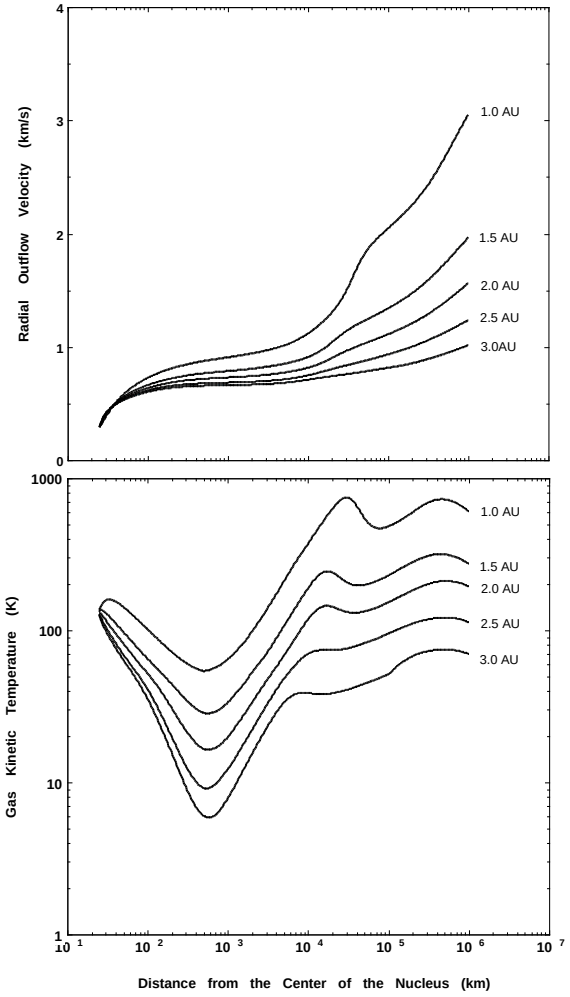

Fig. 2 Kinetic temperature and expansion velocity of a cometary atmosphere as a function of distance to nucleus, for various heliocentric distances, from a 1-D spherical hybrid kinetic/dusty-gas hydrodynamical model (from Combi et al. 1999). The model is applied here to comet C/1995 O1 (Hale-Bopp), with water production rates varying from 4×10^{29} s^{-1} at 3 AU to $8\times10^{30}s^{-1}$ at 1 AU. Other examples may be seen in Combi et al. (2005).

3 Composition and Chemistry

3.1 Vertical structure

Table 1 lists the main gases found in planetary atmospheres in our solar system. As previously mentioned, one may hence subdivide the planets and moons into families of those with N_2 atmospheres, CO_2 atmospheres and H_2/He atmospheres. One may vertically subdivide each atmosphere into two main regions, the homosphere and heterosphere. In the homosphere gases are mixed by turbulent diffusion and their abundances controlled by chemistry, while in the heterosphere the mean free path between gas molecules becomes sufficiently large for molecular diffusion to dominate the vertical gas distribution. In the heterosphere gases tend to adopt a vertical distribution according to their individual scale heights, thus separating from one another. Heavy gases in the heterosphere accumulate at lower altitudes, while the lighter gases become dominant at higher altitudes. The region separating the heterosphere and homosphere is referred to as the homopause. Mathematically speaking the homopause is the altitude/pressure where the eddy and molecular diffusion coefficients are equal, however this criterium has to be treated with caution since other dynamical effects not necessarily captured by the eddy diffusion coefficient (such as global scale dynamics and atmospheric escape) further influence the vertical distribution of gases and thereby the homopause location. The hompopause may rather be regarded as a transition region (as opposed to a specific altitude/pressure) in which the vertical distribution of a given gas changes from being described by the overall atmospheric scale height to being described by its individual scale height. Since the mixing ratios of heavy constituents begin to decrease significantly near the homopause, the chemistry in the heterosphere becomes considerably simpler than at lower altitudes.

The homopause usually lies within the lower thermosphere, which energetically is a natural consequence. Heavy molecules and those efficient in radiatively cooling the atmosphere for reasons outlined above tend to decrease in mixing ratio significantly near the homopause or below, so above the homopause the atmospheric temperatures tend to rapidly increase with altitude, a distinct feature of the lower thermosphere region. On Earth the average homopause is typically located near 105 km altitude (100 nbar) and principal gases above that region are O, N_2 and O_2. On Mars the homopause lies near 125 km (1 nbar), on Venus near 135 km (10 nbar), on both planets principal gases above the homopause being O, CO_2 and N_2. The CH_4 homopause on Jupiter is located near the 10 μbar and on Saturn near 1 μbar level, above which the dominant gases are H, H_2 and He. Recent observations of Titan's upper atmosphere by the Cassini Ion Neutral Mass Spectrometer (INMS) have placed the CH_4 homopause there near 850 km (1.6 nbar) (Yelle et al., 2008), above which the dominant gases are CH_4, N_2 and H_2.

While molecular diffusion is dominant above the homopause, thermospheric dynamics may play a key role in redistributing gases. As first proposed for Earth by Duncan (1969) and later calculated amongst other by Rishbeth and Mueller-Wodarg

(1999), vertical winds in particular affect the distribution of gases, enhancing the abundances of heavier constituents in regions of upwelling and lighter constituents in regions of downwelling, a process also sometimes referred to as ”wind-induced diffusion”. The effects of this are particularly strong in the Earth’s auroral regions where local Joule and particle precipitation heating generate regions of strong upwelling and downwelling, reducing and increasing the O/N_2 ratios locally (Rishbeth and Mueller-Wodarg, 1999). This principle is also responsible for many of the upper atmospheric changes observed during geomagnetic storms, via changes in the O/N_2 ratio, which in turn, via recombination processes, controls ionospheric electron densities. On Venus the nightside hydrogen bulge first observed by the Pioneer Venus spacecraft (Brinton et al., 1980) is believed to be caused by the downwelling as well. The vertical wind redistribution of constituents is believed to act equally on Jupiter (Bougher et al., 2005), Saturn (Mueller-Wodarg et al., 2006a) and Titan (Mueller-Wodarg et al., 2003), although for these atmospheres observations yet have to unambiguously confirm the process happening.

3.2 Composition and evolution

The atmospheric composition of a planet or satellite originates from two primary sources, outgassing of volatiles trapped in the icy grains and/or planetesimals that formed the primary body, and material accumulated via accretion or impact of small bodies during or after the differentiation of the primary body. Such a case is quantitatively developed for the evolution of Earth’s atmosphere by Dauphus (2003), who invokes fractionated nebular gases and accreted cometary volatiles. The fractionation stage resulted in a high Xe/Kr ratio, with xenon being more isotopically fractionated than krypton. Comet-delivered volatiles having low Xe/Kr ratios and solar isotopic composition. The resulting atmosphere had a near solar Xe/Kr ratio, almost unfractionated krypton delivered by comets, and fractionated xenon inherited from the fractionation episode. Similar arguments can be made for Mars based on the noble gas abundances and their isotopic ratios as measured by Viking and from ground based analysis of SNC meteorites (Owen et al., 1992; Bogard et al., 2001). Venus on the other hand shows a distinct difference: the abundances of neon and argon per gram of planet are excessively high (Owen et al., 1992). This must be considered in the context that the Venusian noble gas inventory is less sampled given the lack of a SNC analog. However, for the most part the noble gas inventories of the terrestrial planets (Venus, Earth, and Mars) indicate a similar origin and evolution.

The gas giants have two distinct evolutionary differences. Although they started from similar planetesimal fragments, once they reached a critical size they began to gravitationally accrete protosolar nebular gases (H, He, and Ne) in copius quantities. Furthermore, their distance from the protosun resulted in bombardment by a continuous stream of icy grains whose formation temperatures were below 50 K (Atreya et al., 1999; Owen, 2007). The primary evidence for a significant contribution of

heavy elements in the form of icy grains comes from the super solar ratios (4 ± 2) of argon, krypton, and xenon as well as carbon and sulfur bearing volatiles measured by the Galileo probe in its descent through the Jovian atmosphere, thus the name Solar Composition Icy Planetesimals (SCIPs) (Owen, 2007).

Owen (2007) argues that the abundances of nitrogen and carbon in planetary atmospheres show a similar trend throughout the solar system (15-20 times solar) largely due to the fact that the carbon is easily converted into refractory materials via solar extreme ultraviolet / energetic particle induced chemistry in the interstellar medium, whereas the primary carrier of nitrogen is the highly volatile N_2 molecule requiring cold temperatures for retention on silicate/mineral surfaces. This is most directly illustrated at Venus where the carbon and nitrogen volatile inventory appears to still be present in the atmosphere today. Earth's nitrogen-dominated atmosphere is largely attributed to the creation and burial of carbonates a process mediated by the liquid water in the oceans (apparently absent at Venus). This C/N ratio also implies that for Mars with a CO_2 dominated atmosphere there cannot be large deposits of carbonates or the atmosphere would be predominantly nitrogen - the exception would be if significant burial of nitrogen bearing minerals occurs as well. The domination of N_2 in Titan's atmosphere again suggest the loss of copius quantities of carbon via methane escape (Strobel, 2008a) and/or the conversion of carbon to heavy refractory compounds that are sequestered on Titan's surface (Lorenz, 2008), based on radar observations of surficial features (methane seas and organic dunes). However, both nitrogen in the form of a water-ammonia ocean and methane bound in clathrates may be significant sources of carbon and nitrogen yet accounted for. This is backed up by the amount of ^{40}Ar in the atmosphere (mixing ratio $4.3\pm0.1\times10^{-5}$) equivalent to $\sim$2% outgassing of the interior (Niemann et al., 2004; Waite et al., 2005).

Water is the primary form in which oxygen (and substantial amounts of hydrogen) is found throughout the solar system, although the degree that it exists as vapor is highly dependent on the planet and the temperature of the body. Venus' high D/H ratio in both water and molecular hydrogen gas found in the atmosphere as well as its proximity to the sun are primary arguments for the escape of much of Venus' water to space over geological time (Donahue 1999). Earth's water is largely sequestered in its oceans. Mars' small size and weak gravitational binding of its atmosphere have been used to argue for significant loss of H, C, N, and O to space over geological time (Owen et al., 1992). However, the discovery of increasing quantities of sub-surface water at high latitudes leaves the question open as to how much water has been lost and how much retained in the interior and the polar caps.

The abundance of water in the outer solar system is a question of significant importance. The Galileo entry probe did not measure a super solar abundance of water as it did for carbon and sulfur. However, at the highest pressures measured the water mixing ratio was still rising. This as well as similar altitude dependent variations for sulfur and carbon bearing volatiles has led theorists to postulate that the probe landed in a 5 micron hotspot with a significant downdraft that led to an anomalous altitude distribution of volatiles and that future measurements must sample below this level to determine the water content of Jupiter (Atreya et al., 1999). This is a key

factor for determining whether the SCIP delivery of heavy elements (water should be 4 ± 2 times solar) is correct or whether the heavy elements were delivered in the form of clathrates (water should be $\sim$10 times solar).

In addition to N_2, CO_2 (inner solar system), CH_4 (outer solar system) and H_2O (see Table 1), each of the planets and satellites have their own unique sources of minor volatile compounds that provide important clues to the chemical evolution of the atmosphere. Venus' clouds contain a host of acidic compounds (HCl, HF, H_2SO_4) as well as OCS, SO, SO_2, and CO all presumably derived from late volcanic outgassing in an environment where there is no ocean to mitigate the chemistry (see Table 1 of de Bergh et al., 2006). Viking found both O_2 and CO in the atmosphere of Mars (Owen et al., 1977) - photochemical products of CO_2 photolysis. However, more recently CH_4 has been tentatively detected at the tens of parts per billion level (Formisano et al., 2004, Krasnopolsky et al., 2004; Krasnopolsky, 2007) suggesting either an internal geological process such as serpentinization or perhaps evidence for life in the interior, but the detection is as yet still controversial. Earth has a host of minor hydrocarbon volatiles that are byproducts of biology and many of which are human-induced pollutants largely due to our every increasing appetite for energy.

Jupiter's and Saturn's atmospheres contain the condensable volatiles NH_3, H_2S, as well as H_2O and their by products (i.e., NH_4SH). These gas giant atmospheres also contain a plethora of minor hydrocarbons derived from CH_4 including CH_3, C_2H_2, C_2H_4, C_2H_6, C_3H_4, C_3H_8, C_4H_2, and C_6H_6 (see Table 1 of Atreya et al., 2002). The induced hydrocarbon complexity is especially prevalent at high-latitudes where energetic particle precipitation from the powerful planetary aurorae leads to the formation of polycyclic aromatic hydrocarbons (PAHs) (Wong et al., 2000). This hydrocarbon complexity is also exemplified in the atmosphere of Titan where C_2H_2, C_2H_4, C_2H_6, C_3H_4, C_3H_6, C_4H_2, C_6H_6, and C_2N_2 have been observed (see Table 1 of Waite et al., 2005 and Table 1 of Waite et al., 2007). In fact the relative lack of hydrogen (for recombination with the photochemical initiator CH_3 to reform CH_4) as compared to Jupiter and Saturn, combined with the existence of N_2 and sufficient sources of free energy from solar extreme ultraviolet and energetic particle precipitation provide a unique environment at 1000 km above Titan's surface for the initiation of ion neutral chemistry that reaches complexities of over 10,000 atomic mass units (Waite et al., 2007) and contains a host of nitrile compounds (HCN, HC_3N, C_2H_3CN, CH_2NH, CH_3CN, C_2H_5CN, CH_3C_3N, HC_5N, C_5H_5N, CH_3C_5N, and C_6H_7N) (Vuitton et al., 2007) as well as the hydrocarbons cited above. This chemistry appears to have similar character and complexity to processes in interstellar clouds apart from the substitution of predominantly nitrogen bearing compounds for the oxygenated hydrocarbons of interstellar clouds. The large negative ions formed via this process are postulated as the precursor of the organic haze found throughout Titan's atmosphere.

In summary, the noble gases and their isotopic ratios are the best way to compare the origin and evolution of the volatiles that make up an atmosphere. The predominant form of carbon is CO_2 for the inner planets and CH_4 at the outer planets. Oxygen and hydrogen in the form of water is found at all the planets and satellites. However, the uncertainty of the water content of the outer solar system planets is a

major open issue in our understanding of planetary formation. Nitrogen is primarily in the form of N_2 in the inner solar system and NH_3 in the outer solar system with the exception of Titan, which has a thick N_2 atmosphere. Minor species are involved in cloud and haze formation and can tell us much about the chemical evolution of the atmosphere.

3.3 Atmospheric chemistry

The middle and upper atmospheres of planets in our solar system are cold enough that thermochemical equilibrium tends to play a negligible role in controlling atmospheric composition. Instead, aeronomy in these regions is dominated by disequilibrium photochemistry and chemical kinetics. Atmospheric chemistry is initiated when atoms or molecules absorb solar ultraviolet photons and/or when they interact with charged particles from the solar wind or planetary magnetospheres; that chemistry can in turn affect many properties of the atmosphere. For example, catalytic chemical cycles can allow trace photochemical constituents to profoundly affect the composition and properties of the bulk atmosphere, such as with odd-hydrogen chemistry maintaining carbon dioxide on Mars or chlorine chemistry influencing the composition of the middle atmospheres of Venus and the Earth. Trace photochemical constituents can also profoundly affect radiative balance and energy transport in an atmosphere, which in turn can affect atmospheric thermal structure and dynamics, such as with hydrocarbon photochemical products controlling radiative transport on the giant planets and Titan. Understanding the quantitative details of the chemical production and loss of minor species in a planetary atmosphere is therefore important for fully understanding the behavior of planetary atmospheres.

3.3.1 Terrestrial planets

The chemistry of the middle and upper atmosphere of the Earth is too broad a subject to be effectively covered in this short review. Seinfeld and Pandis (2006), Brasseur and Solomon (2005), Wayne (2000), Finlayson-Pitts and Pitts (2000), and Brasseur et al. (1999) provide good general reviews of the subject.

Photochemistry on Mars is not completely understood. Many of the basic processes have been worked out, but current photochemical models have difficulty simultaneously reproducing the observed abundances of O_2, CO, H_2O_2, O_3, H_2O and H_2, indicating shortcomings with the models (e.g., Nair et al. 1994, Atreya and Gu 1994, Krasnopolsky 1995). Global-average one-dimensional (1-D) models have now been augmented by time-variable 1-D models (e.g., Clancy and Nair 1996, García Muñoz et al. 2005, Krasnopolsky 2006a, Zhu and Yee 2007) and by multidimensional photochemistry-transport models (e.g., Moreau et al. 1991, Lefèvre et al. 2004, Moudden and McConnell 2007, Moudden 2007), which can better explain

some of the seasonal, diurnal, and spatial variability of atmospheric constituents, but some puzzles still remain.

The Martian atmosphere is composed predominantly of CO_2, which can be photolyzed by solar ultraviolet photons to produce CO and O. The recombination of CO and O is spin forbidden and very slow. The oxygen atoms will instead combine with other oxygen atoms to form O_2. Large amounts of CO and O_2 in a 2:1 ratio would be expected to form in a pure CO_2 atmosphere. The Martian atmosphere is not pure CO_2, however, and McElroy and Donahue (1972) and Parkinson and Hunten (1972) first pointed out the fundamental importance of catalytic cycles involving the so-called "odd hydrogen" HO_x species (e.g., H, OH, HO_2), which together with H_2O_2 help recycle the CO_2 and reduce the CO and O_2 abundances (and the CO/O_2 ratio) on Mars. Water photolysis, along with the reaction of H_2O with $O(^1D)$ from CO_2, O_2, and O_3 photolysis, provides the source of the HO_x species. One important HO_x catalytic cycle is

$$\begin{aligned} H + O_2 + M &\longrightarrow HO_2 + M \\ O + HO_2 &\longrightarrow O_2 + OH \\ CO + OH &\longrightarrow CO_2 + H \\ \hline \text{Net}: \quad CO + O &\longrightarrow CO_2, \end{aligned}$$

but others involving O_3, H_2O_2, and perhaps odd-nitrogen (NO_x: NO, NO_2) species operate as well (e.g., Krasnopolsky 1986, Yung and DeMore 1999). The HO_x catalytic cycles are so effective at removing CO that photochemical modelers (e.g., Nair et al. 1994, Atreya and Gu 1994, Krasnopolsky 2006a) have resorted to invoking heterogeneous reactions on aerosol surfaces or changes in measured reaction rate coefficients as a means of reducing HO_x abundances in order to reproduce the observed CO abundance on Mars. Note that no measurements of O densities have to-date been published for Mars.

HO_x chemistry also strongly affects the abundance of many other atmospheric species, including O_3, H_2O_2, and H_2. The photochemistry of ozone on Mars is discussed by Lefèvre et al. 2004 and references therein. Ozone is produced through three-body recombination of O with O_2 and is lost through reactions with HO_x species. Because HO_x species are derived from water photochemistry, an anticorrelation between O_3 and H_2O abundances is expected (e.g., Clancy and Nair 1996), although the actual O_3-H_2O relationship becomes more complicated than this simple picture when full seasonal, meridional, and vertical variations are taken into account (e.g., Lefèvre et al. 2004, 2007; Krasnopolsky 2006a). Dayglow observations from the $a\,^1\Delta_g \rightarrow X\,^3\Sigma_g^-$ electronic transition of O_2 have also been used as a proxy to track ozone abundances, and $O_2(a\,^1\Delta_g)$ chemistry is usually included in photochemical models (e.g., García Muñoz 2005, Krasnopolsky 2006a). The chemistry of H_2O_2, which is observed to vary with location and season on Mars (e.g., Encrenaz et al. 2004), has been extensively studied. Hydrogen peroxide is produced mainly through reaction of HO_2 with HO_2 and is lost through photolysis. Because H_2O_2

is derived from HO_x chemistry, the abundances of H_2O and H_2O_2 are expected to be correlated to some extent (e.g., Krasnopolsky 2006a, Moudden 2007), although again complications with this correlation are present in observations and models. HO_x species and O_3, $O_2(a^1\Delta_g)$, and H_2O_2 are all short-lived enough that diurnal variations in abundances are expected.

Molecular hydrogen, on the other hand, is long-lived on Mars. Water dissociation provides a source of atomic H, and reaction of H with HO_2 produces H_2. The long-lived H_2 molecules can then diffuse into the upper atmosphere where ion reactions convert H_2 back into H, and the H can escape. Hydrogen chemistry on Mars is a classic example of chemical coupling between the upper and lower atmospheres, and the bulk Martian atmospheric composition cannot be understood without examining the behavior of the entire atmosphere, from the surface to the exobase. Hydrogen escape over time could potentially affect the oxidation state of the Martian atmosphere; however, nonthermal escape mechanisms for oxygen also exist (as well as potential surface sinks of reactive oxygen), and the Martian atmosphere may be self-regulating in the sense that a steady-state loss of two hydrogen atoms for every one oxygen atom is maintained (see Yung and DeMore 1999 for further details), although this has to-date not yet been proven to be the case on Mars.

The recent tentative detection of CH_4 on Mars (Formisano et al. 2004, Krasnopolsky et al. 2004, Krasnopolsky, 2007) has sparked much interest due to potential astrobiological implications and due to a puzzling observed variability with time and location, but much uncertainty still surrounds this detection. Methane is expected to have a relatively long ($\sim$300-700 year) photochemical lifetime on Mars (Wong et al. 2003, Krasnopolsky et al. 2004) — short-term temporal and spatial variability is therefore unexpected, and a significant source must exist to replace loss by photolysis and reaction with OH, O, and $O(^1D)$. Although it is possible that some hitherto unidentified photochemical production mechanism may exist in the Martian atmosphere (Bar-Nun and Dimitrov 2006) or that the methane is derived from meteoroid impacts, it is more likely that the methane derives from crustal or interior sources (e.g., fluid-rock interactions, volcanism, methane clathrate hydrates, methanogenic bacteria; e.g., Max and Clifford 2000, Krasnopolsky et al. 2004, Oze and Sharma 2005, Lyons et al. 2005, Krasnopolsky 2006b, Atreya et al. 2007). The observed temporal variability suggests that local surface sources and sinks could be operating.

Venus, with its massive CO_2 atmosphere, shares some similarity in atmospheric chemistry with Mars, but the catalytic removal of CO and O_2 to recycle the CO_2 atmosphere is apparently considerably more efficient on Venus than on Mars. Early photochemical models (e.g., Winick and Stewart 1980, Yung and DeMore 1982, Krasnopolsky and Parshev 1983) overpredicted the O_2 abundance and underpredicted the efficiency of CO_2 recycling. Aside from the HO_x catalytic cycles described for Mars, chlorine catalytic cycles, such as the following, likely operate to stabilize CO_2 on Venus:

$$\mathrm{Cl + CO + M \longrightarrow ClCO + M}$$
$$\mathrm{ClCO + O_2 + M \longrightarrow ClC(O)O_2 + M}$$

$$\begin{array}{l} \mathrm{ClC(O)O_2 + O \longrightarrow CO_2 + O_2 + Cl} \\ \hline \mathrm{Net:\ \ CO + O \longrightarrow CO_2,} \end{array}$$

where the chlorine atoms are derived from HCl. The chlorine cycles are expected to have much more influence than the HO_x cycles on Venus. The above cycle, first proposed by Yung and DeMore (1982), is used in more recent photochemical models, along with oxidation of CO on cloud particles, to help explain the efficiency of CO_2 recycling on Venus (e.g., Pernice et al. 2004, Mills et al. 2006, Mills and Allen 2007), but significant uncertainties remain in the details of the CO_2 cycle on Venus. Slanger et al. (2006) have proposed that reaction between excited $O_2(c\,^1\Sigma_u^-, v = 0)$ and CO may help explain both the CO_2 stability and an observed variability of 557.7 nm oxygen green line emission and 1.27-μm $O_2(c - X)$ emission on Venus.

Thermochemical equilibrium and high-temperature kinetic processes prevail in the lowest regions below the cloud decks on Venus (e.g., Krasnopolsky 2007). Near $\sim$60 km (i.e., the upper cloud region), SO_2 is oxidized through photochemical processes to form H_2SO_4, which condenses and falls to lower altitudes, where it thermally decomposes to produce SO_2 and H_2O. This sulfur oxidation cycle may be influenced by coupled CO and SO_2 oxidation, whose net result is CO + SO_2 + O_2 + H_2O $\longrightarrow$ CO_2 + H_2SO_4 (e.g., Yung and DeMore 1982, 1999). An up-to-date discussion of the unknown cloud constituent that absorbs at blue wavelengths is provided by Krasnopolsky (2006c). The chemistry of sulfur in the Venus atmosphere is rich and complex, and other interesting sulfur cycles besides SO_2 oxidation may exist, including coupled chlorine and sulfur chemistry (e.g., DeMore et al. 1985, Mills 1998, Mills and Allen 2007) and elemental sulfur ("polysulfur") cycles (e.g., Krasnopolsky and Pollack 1994, Mills 1998, Yung and DeMore 1999). Nitrogen chemistry on Venus has also been examined, and NO_x chemistry has the potential to affect the major photochemical products (e.g., Yung and DeMore 1999). Atmospheric dynamics likely affects photochemical processes on Venus, but multidimensional coupled chemical-dynamical models of the lower and middle atmosphere of Venus have yet to be developed.

The neutral upper atmosphere of Venus is affected by ionospheric chemistry, solar-cycle variations, dynamics, and escape. Nonthermal escape processes such as charge exchange, sputtering, solar-wind pick up, detached plasma clouds, and collisional ejection (via hot-atom production during photochemical reactions) dominate over thermal escape (see Lammer et al. 2006). The review by Fox (2004) discusses recent advances related to the aeronomy of the Venusian thermosphere (see also the older reviews of Fox and Bougher 1991, Fox and Sung 2001).

Although our understanding of atmospheric chemistry on Venus has advanced greatly in the past three decades, numerous outstanding questions remain (e.g., Mills and Allen 2007, Krasnopolsky 2006c). Venus Express data will hopefully provide new key measurements on the three-dimensional distribution of atmospheric constituents, maps of airglow emission, temperature retrievals, and wind derivations that will improve our understanding of chemical and physical processes in Venus'

atmosphere. First measurements by the Spectroscopy for Investigation of Characteristics of the Atmosphere of Venus (SPICAV) instrument of minor mesospheric constituents and an unexpected warm layer near 100 km on the nightside have been reported by Bertaux et al. (2007). Mesospheric emissions in the infrared by CO_2 (non-LTE at 4.3 μm on the dayside) and O_2 (1.27 μm on the nightside) have been observed by the Venus Express Visible and Infrared Thermal Imaging Spectrometer (VIRTIS) (Drossart et al., 2007). These data, combined with much-needed laboratory experiments, theoretical models, and continued Earth-based observations will provide vital clues for deciphering the remaining questions regarding the intricate chemical coupling mechanisms in the Venus atmosphere.

3.3.2 Giant planets

The hydrogen-dominated giant planets Jupiter, Saturn, Uranus, and Neptune share many similarities in upper-atmospheric chemistry, although some notable differences exist. Temperatures are low enough on the giant planets that major equilibrium volatiles like H_2O, NH_3, and H_2S will condense in the tropospheres of all the giant planets, and even CH_4 will condense on Uranus and Neptune. Methane, the most volatile of all these major hydrides, can survive past the tropopause cold trap and be transported to the upper stratosphere or mesosphere, where it will interact with solar and stellar ultraviolet radiation and be photodissociated. Methane photochemistry therefore dominates middle-atmospheric chemistry on the giant planets, and the major photochemical products are complex hydrocarbons. Molecular diffusion of the relatively heavy methane molecules in the lighter background hydrogen gas eventually limits the vertical extent to which the CH_4 can be carried on the giant planets and provides a natural boundary between the middle atmosphere and thermosphere. The long-lived hydrocarbon photochemical products eventually diffuse down into the deep troposphere, where they are thermochemically converted back to methane, completing the methane cycle. Uranus' weak internal heat source (unlike that of the other giant planets) seems to suppress vertical motions, allowing molecular diffusion to take over at relatively low altitudes and preventing the buildup of the large column abundances of complex hydrocarbons that are observed on the other giant planets.

Our current understanding of hydrocarbon photochemistry on the giant planets is reviewed by Strobel 2005, Moses et al. 2004, and Yung and DeMore 1999. Further details of the photochemistry on each giant planet can be found in models presented by Romani and Atreya 1988, Summers and Strobel 1989, Romani et al. 1993, Gladstone et al. 1996, Romani 1996, Bishop et al. 1998, Moses et al. 2000a, 2005, Lebonnois 2005, and Moses and Greathouse 2005. Methane is photolyzed predominantly by Lyman α photons at 121.6 nm, and the major photolysis products are CH_3, $CH_2(a^1A_1)$, and CH. The methane photolysis branching ratios at 121.6 nm are not completely known. The CH_3 radicals will either recombine with themselves to form C_2H_6, or combine with H to reform methane. $CH_2(a^1A_1)$ radicals will react with H_2 to either produce CH_3 or to quench to the ground state and eventually react

with H to form CH. The CH radicals can insert into methane to form C_2H_4, into ethane to form C_3H_6, or into H_2 to recycle CH_2.

The major hydrocarbon photochemical products on the giant planets are ethane (C_2H_6), acetylene (C_2H_2), ethylene (C_2H_4), propane (C_3H_8), methylacetylene (C_3H_4), diacetylene (C_4H_2), benzene (C_6H_6), and methyl radicals (CH_3), all of which have been observed on one or more of the giant planets. The primary mechanisms for producing complex hydrocarbons are radical-radical combination reactions (e.g., $2CH_3 + M \longrightarrow C_2H_6 + M$), CH insertion reactions (e.g., $CH + CH_4 \longrightarrow C_2H_4 + H$), and C_2H insertion reactions (e.g., $C_2H + C_2H_2 \longrightarrow C_4H_2 + H$). Photolysis, cracking by atomic hydrogen (e.g., $H + C_2H_5 \longrightarrow 2CH_3$), and disproportionation reactions (e.g., $CH_3 + C_3H_2 \longrightarrow C_2H_2 + C_2H_3$) are the primary mechanisms for destroying carbon-carbon bonds. Atomic hydrogen is a major product of this hydrocarbon photochemistry, and reactions of H with hydrocarbons are of critical importance in defining the relative abundances of the major constituents. Ethane and acetylene are major coolants in giant-planet stratospheres, and photochemistry therefore strongly influences the atmospheric thermal structure (e.g., Bézard and Gautier 1985, Yelle et al. 2001). Although hydrocarbon photochemistry on the giant planets is qualitatively understood, some quantitative details are lacking, especially for the photochemistry of C_3H_x hydrocarbons and benzene. Laboratory measurements and theoretical calculations are needed to fill in uncertain model parameters and uncertain spectroscopic parameters for abundance derivations (see also Huestis et al., 2008).

The recent detection of oxygen compounds that are unambiguously in the stratospheres of the giant planets (aside from the Comet Shoemaker-Levy 9 impact debris on Jupiter) indicates that external material from meteoritic dust, ring/satellite debris, and/or cometary impacts frequently enters giant-planet atmospheres (e.g., Feuchtgruber et al. 1997, 1999; Bergin et al. 2000; Moses et al. 2000b; Bézard et al. 2002; Lellouch et al. 2002, 2005, 2006; Kunde et al. 2004; Flasar et al. 2005a; Burgdorf et al. 2006; Hesman et al. 2007). The relative importance of each of these sources is not well understood and may differ from planet to planet. The influx of oxygen species can have a minor effect on hydrocarbon abundances (e.g., Moses et al. 2000b, 2005). Water derived from external sources will condense in the stratospheres of all the giant planets and contribute to the stratospheric haze load. Above the condensation region, water is lost primarily by photolysis to form OH + H, but the OH reacts with H_2, CH_4, and C_2H_6 to efficiently recycle H_2O. Some of the water can be permanently converted to other oxygen compounds (mainly CO) through three-body addition of OH with C_2H_2 and C_2H_4, which forms complexes that eventually produce CO. These reactions of OH with unsaturated hydrocarbons most likely dominate over $O + CH_3$ or $OH + CH_3$ in the photochemical production of CO on the giant planets (Moses et al. 2000b, 2005). CO is quite stable in giant-planet stratospheres and will be lost through diffusion into the troposphere. Carbon dioxide can form through the reaction of $OH + CO \rightarrow CO_2 + H$. Interestingly, the large CO abundance on Neptune and the vertical distribution of that CO suggest that Neptune may have experienced a large cometary impact on the order of 200 years ago (Lellouch et al. 2005; see also Hesman et al. 2007). Between this event, and the 1994 Shoemaker-Levy 9 impacts with Jupiter, the fate of cometary debris on

the giant planets is of great interest not only for understanding current atmospheric chemistry on the giant planets but for understanding impact rates in the solar system.

Observers have now mapped the meridional distribution of several stratospheric constituents on Jupiter and Saturn (e.g., Kunde et al. 2004, Flasar et al. 2005a, Greathouse et al. 2005, Prange et al. 2006, Nixon et al. 2007, Howett et al. 2007), and the observations indicate the need for coupled photochemistry-transport models (see Moses and Greathouse 2005, Liang et al. 2005, Lellouch et al. 2006, Moses et al. 2007). Another focus of current research is the extent to which auroral chemistry affects the stratospheric composition locally and perhaps even globally on Jupiter and Saturn (e.g., Wong et al. 2000, 2003; Friedson et al. 2002). Outstanding problems include the underlying reasons for the differences in the hydrocarbon abundances on the giant planets, the underlying physical and chemical mechanisms controlling the meridional distribution of hydrocarbons on the giant planets, the details of the intricate coupling between chemistry, temperatures, and dynamics on the giant planets, and the reasons for the observed changes in composition over time.

3.3.3 Titan, Pluto, Triton, and Io

Atmospheric chemistry on Titan is vigorous and complex and understood only in its basics. As on the giant planets, hydrocarbon photochemistry plays a large role in the middle and upper atmosphere, but Titan is composed predominantly of N_2 rather than H_2, and the resulting photochemistry differs considerably. On the giant planets, the dominant nitrogen-bearing constituent — in this case NH_3 — is physically separated from the methane photolysis region due to tropospheric condensation. Coupled carbon-nitrogen chemistry is therefore suppressed on the giant planets (although Neptune, which may contain a large amount of N_2, is an exception, see Lellouch et al. 1994). That is not the case on Titan. On Titan, as on the Earth, N_2 can be dissociated at high altitudes. Although 127 nm photons have sufficient energy to break the strong N_2 bond, N_2 photoabsorption only becomes significant at wavelengths below 100 nm, and photolysis occurs indirectly through excitation into predissociating electronic states, which provides only a minor source of N atoms. Instead of direct photolysis, the N_2 bond is broken predominantly through dissociative ionization from impacting magnetospheric electrons or solar EUV photons. The ultimate products of this process are $N(^2D)$, N, and N^+. The N atoms can react with CH_3 to produce H_2CN, and eventually HCN and other nitriles (e.g., through dissociation of HCN to CN, followed by reaction of CN with unsaturated hydrocarbons like C_2H_2 and C_2H_4 to form HC_3N and C_2H_3CN, respectively). The N^+ ions also can react with methane and follow subsequent pathways that can lead to nitrile production. The excited $N(^2D)$ atoms can react with CH_4 to produce NH, which predominantly ends up recycling the N_2. $N_2{}^+$ ions can also react with methane to produce $CH_3{}^+$ or $CH_2{}^+$ ions, followed by ion-neutral reactions to produce complex hydrocarbon ions, which can recombine with electrons to produce complex neutral hydrocarbon molecules.

The suggestion that ion chemistry has a significant impact on Titan's neutral atmospheric chemistry (e.g., Banaszkiewicz et al. 2000, Molina-Cuberos et al. 2002, Wilson and Atreya 2004) and aerosol formation has been dramatically demonstrated from measurements acquired with the Ion-Neutral Mass Spectrometer (INMS) aboard the Cassini spacecraft (e.g., Waite et al. 2005, 2007; Cravens et al. 2006; Vuitton et al. 2006, 2007) and is further confirmed from laboratory experiments (e.g., Imanaka and Smith 2007). The production of nitriles, polycyclic aromatic hydrocarbons (PAHs), and "tholins" in particular may be augmented by ion chemistry.

Hydrocarbon photochemistry in Titan's middle atmosphere is very similar to that described above for the giant planets, with some minor differences resulting from the fact that H_2 is much less abundant on Titan, and hydrogen escape affects abundances (see Yung et al. 1984, Toublanc et al. 1995, Lara et al. 1996, Yung and DeMore 1999, Wilson et al. 2003, Wilson and Atreya 2004, and Lebonnois 2005 for detailed descriptions of Titan photochemistry). Unlike the giant planets, however, there is no obvious mechanism for converting the complex hydrocarbons back to methane. Methane will be irreversibly destroyed by photochemistry on a time scale of $\sim$10-100 million years in Titan's atmosphere, and the complex hydrocarbon products will rain down or diffuse onto the satellite surface. The fact that methane is still present in Titan's atmosphere suggests either that the human species observe Titan at a point of time where much of its methane is still present in the atmosphere or, more likely, that a significant surface or interior source mechanism must exist. Similar to what has been suggested for methane production on Mars, several hydrogeochemical sources are possible (e.g., Atreya et al. 2006). As on the giant planets, the presence of H_2O in Titan's upper atmosphere suggests an external source of oxygen (Coustenis et al. 1998). The photochemistry of oxygen species in Titan's atmosphere is discussed by Wong et al. 2002 and Wilson and Atreya (2004). Coupled photochemistry-dynamical models have recently been developed for Titan to help explain observed meridional and seasonal variations in species abundances (e.g., Lebonnois et al. 2001, Luz et al. 2003).

Many outstanding problems regarding neutral atmospheric chemistry on Titan remain, including details of the complex ion-neutral coupling, the pathways that convert gas-phase species to "tholins" and other aerosols, the dominant physical and chemical mechanisms controlling the latitude, altitude, and time variation of hydrocarbons and nitriles, the evolutionary history of atmospheric chemistry on Titan, the source of methane, the origin and fate of oxygen species, and the mechanisms and rates or escape of atmospheric constituents.

Pluto and Triton have vapor-pressure-controlled atmospheres composed largely of N_2, CO, CH_4, and Ar that are buffered by surface ices. The atmospheric photochemistry on Pluto and Triton is expected to be similar and share some general characteristics with hydrocarbon, nitrogen, and oxygen photochemistry on Titan. Methane is expected to produce hydrocarbons like C_2H_2 and C_2H_6, which would condense to form hazes. Coupled N_2-CH_4 photochemistry can produce nitriles, which would also condense. The presence of abundant CO adds some interesting atomic carbon chemistry that differs from the situation on Titan. Ion chemistry is again intimately linked with neutral chemistry. Atmospheric escape is prevalent. For

details concerning atmospheric chemistry on Pluto and Triton, see Strobel and Summers (1995), Krasnopolsky and Cruikshank (1995, 1999), Summers et al. (1997), Lara et al. (1997), Yung and DeMore (1999).

Io's atmosphere is also buffered by surface frosts, but in this case by SO_2. Carbon and hydrogen appear to be virtually absent from the system, so Io's atmospheric chemistry is unique in the solar system. Volcanism is the ultimate source of the SO_2, and active volcanic outgassing may locally affect atmospheric chemistry. The SO_2 atmosphere as a whole appears to be dominated by frost sublimation (e.g., Jessup et al. 2004, Saur and Strobel 2004, Strobel and Wolven 2001), except at high latitudes and near the terminators (e.g., at high solar zenith angles) or on the night side, where local volcanic regions can be important. Temporal variability is also evident in observations. Sulfur dioxide is dissociated to form SO and O (dominant branch) or S + O_2, and subsequent chemistry produces an atmosphere in which SO_2, SO, O, S, and O_2 dominate the neutral chemistry. Observations of S_2 at ultraviolet wavelengths (e.g., Spencer et al. 2000, Jessup et al. 2007), NaCl at millimeter wavelengths (Lellouch et al. 2003), and SO emission at 1.7 μm (de Pater et al. 2002, 2007; Laver et al. 2007) indicate that the background atmosphere can be perturbed by active volcanoes. S_2 is short-lived and is readily photolyzed to form S or can react with O to form SO. Other products of S_2-SO_2 photochemistry include S_x species (e.g., S_3, S_4, S_8) and S_2O. Alkali chemistry leads to NaCl, Na, Cl, K, KCl, and perhaps species such as $NaSO_2$.

Details of SO_2 photochemistry on Io are discussed by Summers and Strobel (1996), and the influence of volcanic species like S_2 and NaCl are discussed by Moses et al. (2002a, 2002b). These 1-D hydrostatic-equilibrium models are useful for elucidating the dominant chemical production and loss mechanisms on Io but do not provide realistic descriptions the actual atmosphere, in which the SO_2 gas will flow rapidly away from the subsolar point or volcanic sources. Multi-dimensional coupled chemistry-transport models have been developed by Wong and Johnson 1996, Wong and Smyth 2000, Smyth and Wong 2004 (see also Zhang et al. 2003, 2004; Saur and Strobel 2004). Thermochemistry in volcanic gases has been studied by Zolotov and Fegley (1998a, 1998b, 1999, 2000), Fegley and Zolotov (2000), Schaefer and Fegley (2004, 2005a, 2005b, 2005c). The latter papers show that volcanic sources can introduce more exotic species into Io's atmosphere, albeit at minor abundances.

3.3.4 Comets

Except for some limited in situ investigations (e.g., comet Halley with the mass spectrometers of VEGA and Giotto), the chemical composition of comets is assessed by remote sensing. In this investigation, radio and infrared spectroscopy are the main techniques used, since visible and ultraviolet spectroscopy are only sensitive to secondary products radicals, ions and atoms with the notable exception of CO and its UV bands. The current census of these cometary molecules is reviewed by Bockelée-Morvan et al. (2005) and production rates of volatiles shown

in Fig. 3. The major cometary species are probably all known now, but many minor constituents are still to be identified.

The overwhelming chemical process in cometary atmospheres is photolysis, leading to photodegradation and photoionization of the cometary molecules (Huebner et al., 1992; Crovisier, 1994). Hence the paradigm of parent molecules, directly sublimated from nucleus ices, and their degradation product, the daughter molecules (in fact a misnomer, since they are indeed radicals, atoms or molecular ions). Two-body chemical reactions between neutrals have very low rates because of the low temperature and of the energy threshold of such reactions. This is not the case for ion-neutral reactions, but they have little influence on the chemical composition because of the low ionization state of the inner coma (Rogers et al., 2005). Thus it

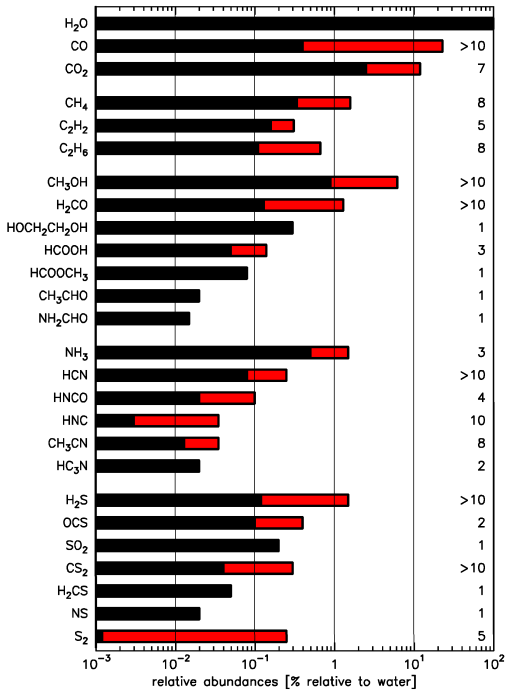

Fig. 3 Production rates of cometary volatile molecules relative to water, in percent. These rates are believed to trace the relative abudances in cometary ices. The grey portions of the bars show the range of the comet-to-comet variations. The number of comets for which data are available is listed on the right. (Adapted and updated from Bockelée-Morvan et al., 2005).

is unlikely that the minor constituents observed in the coma (Fig. 3) result from chemical reactions. They rather come from nucleus ices, or from the degradation of organic grains, the so-called distributed sources.

Photodestruction rates, normalised at 1 AU from the Sun, are typically $\beta = 10^{-6}$ to 10^{-4} s^{-1}. They are 1.3×10^{-5} s^{-1} for water, 2×10^{-6} s^{-1} for a long-lived species such as CO_2, and around 2×10^{-4} s^{-1} for short-lived species such as NH_3, H_2S or SO_2 (Huebner et al., 1992; Crovisier, 1989, 1994). These rates are not yet known with sufficient accuracy for all species, especially for radicals, for which quantitative absorption spectra are difficult to obtain.

Imaging the lines of cometary molecules with radio interferometers, or long-slit spectroscopy in the visible or the infrared, give direct measurements of the molecular space distributions. In this way, one can put stringent constraints to the photodestruction rates, test parent molecule-daughter molecule filiations, and investigate distributed sources. For example, in a study of sulfur-bearing molecules in comet Hale-Bopp with the Institut de Radio Astronomie Millimétrique (IRAM) interferometer, Boissier et al. (2007) obtained interesting constraints to the lifetimes of the CS and SO radicals.

The origin of some radicals is not yet fully understood: this is the case for NS and S_2 which are unlikely to come from nucleus ices or from a parent molecule. In this situation, coma chemistry has been invoked (Canaves et al., 2007). Another puzzling case is that of hydrogen isocyanide HNC (e.g., Lis et al., 2008). Chemical models are unable to account for a HCN$\longrightarrow$HNC conversion. The HNC/HCN abundance ratio is found to increase when the distance to the Sun decreases. This would favour the production of HNC from the thermal degradation of organic grains. Among the major cometary molecules, several bona fide parent molecules are known to come from a significant extended source in addition to the native, nuclear source. This is the case for H_2CO, OCS, CO.

Comets are not all alike. Large variations in the relative molecular abundances are observed from comet to comet. From a dynamical point of view, one distinguishes Jupiter-family comets coming from the Kuiper belt and nearly-ecliptic comets coming from the Oort cloud. If these two main dynamical classes correspond to different formation scenarios, one would expect different chemical compositions (Crovisier, 2007).

The diversity of the chemical composition of comets has been studied for daughter molecules with narrow-band spectro-photometry in the visible (about 100 comets; e.g., A'Hearn et al., 1995), for parent molecules from radio spectroscopy (about 30 comets; Biver et al., 2002) and infrared spectroscopy (about 15 comets; e.g., Mumma et al., 2003). The diversity of relative abundances of parent molecules is indicated in Fig. 3. The scatter is peculiarly large for species such as CO, CH_3OH, H_2CO, H_2S. However, the two main fragments of the split comet 73P/Schwassmann-Wachmann 3 were found to have similar compositions, suggesting that the building blocks of this comet had a uniform composition (Villanueva et al., 2006; Dello-Russo et al., 2007).

From their taxonomic study based upon daughter molecules, A'Hearn et al. (1995) proposed two classes of comets according to their C_2/CN ratio: typical

comets and C_2-depleted comets. The taxonomy studies based upon parent molecules are still in their infancy. There is no obvious link between cometary composition and dynamical origin, except that the C_2-depleted class of comets is found to be linked to Jupiter-family comets (A'Hearn et al., 1995). It is not known how this translates into terms of parent molecules, because the parents of the C_2 radical are still poorly identified.

4 Dynamics and vertical coupling

4.1 Global dynamics and waves on Earth

Atmospheric dynamics can in terms of time be separated into several components, the "mean circulation" which varies on seasonal time scales, the "tidal component" which varies on time scales of a day (rotation) or fractions thereof and the "turbulent component" which describes variations on time scales of small fractions of a rotation (hours to minutes or less). Additionally, one may subdivide dynamics into their geographical extent, namely global (planetary-scale), intermediate (extending over several degrees in latitude/local time) and local (on scales of km or less). This chapter will concentrate on the global mean circulation in planetary atmospheres, describing a summary of the main characteristics of atmospheric dynamics and the importance of atmospheric waves.

Often atmospheric winds are associated with solar heating, but in addition to the thermal drivers of winds there are other momentum sources, including turbulence, wave drag and in the ionosphere/thermosphere region of magnetized bodies ion drag. While particular momentum sources may play a role in specific regions only, the atmosphere is ultimately an integrated and coupled system, whereby conservation of mass and other coupling processes (wave drag, viscosity amongst other) require us to look at an atmosphere as a global entity. Mostly, dynamical coupling occurs upward, so the stratosphere/mesosphere region will affect the thermosphere more than vice-versa. However, this may not be true in terms of composition, where downward flux of gases formed at higher altitudes often plays an important role. A striking example of this is the atmosphere of Titan, where ionospheric chemistry is believed to profoundly affect the composition of the stratosphere and below.

Extensive wind observations have been made on Earth over the past decades using satellites such as the Atmospheric Explorer (AE), Dynamics Explorer (DE), Upper Atmosphere Research Satellite (UARS) and the Thermosphere Ionosphere Mesosphere Energetics and Dynamics (TIMED) satellite as well as rockets, balloons and ground based telescopes. Some of these measurements have been summarized in an empirical model, the Horizontal Wind Model (HWM) which represents a spectral fit to the data (Hedin et al., 1996). Figure 4 shows diurnally and longitudinally averaged zonal winds in the Earth's atmosphere between the surface and

300 km altitude, as given by the HWM for equinox conditions at low geomagnetic and moderate solar activity conditions.

Wind profiles such as these are successfully reproduced also by General Circulation Models (GCMs), including the Coupled Mesosphere and Thermosphere (CMAT) model (Harris, 2000; Harris et al., 2002). This model is one example of codes developed for Earth that reach from the stratosphere to the thermosphere, covering most of the vertical extent of the atmosphere. Another example of such a model is the Thermosphere Ionosphere Mesosphere Electrodynamic General Circulation Model (TIME-GCM) of Roble and Ridley (1994). Development of such models over the past decade was motivated by the recognition that vertical coupling in the atmosphere was important. The need is now recognized to study the atmosphere in its entirety from the lower to the upper atmosphere, rather than examining regions such as the thermosphere in isolation (see also Bougher et al., 2008).

The success of physical models such as CMAT in reproducing observed winds in the stratosphere, mesosphere and thermosphere allows us to investigate the momen-

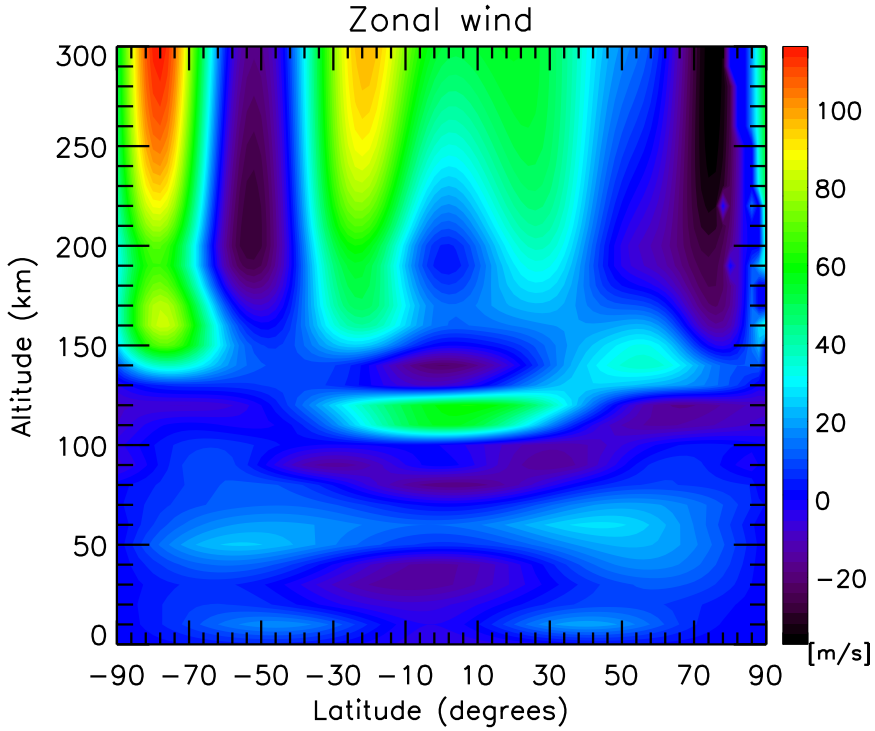

Fig. 4 Diurnally and longitudinally averaged zonal winds (positive eastward) in the Earth's atmosphere, as given by the Horizontal Wind Model (HWM) of Hedin et al. (1996) for equinox conditions at low geomagnetic activity (ap=6) and moderate solar activity (F10.7=100).

tum balance in the Earth's atmosphere. In the stratosphere and mesosphere pressure gradients balance Coriolis forces, resulting in geostrophic flow parallel to isobaric surfaces. The eastward jets in Figure 4 at mid-latitudes near 50 km are driven by stratospheric ozone heating which generates poleward winds (not shown) which become eastward due to Coriolis forces. In the thermosphere the momentum balance is found to be between pressure gradients, Coriolis forces, vertical viscosity and ion drag, giving a much more complex situation that requires numerical models for accurate calculation due to the non-linearity of the problem. Wind flow in the low and mid latitude thermosphere is primarily from the sub-solar to anti-solar hemisphere perpendicular to isobars. At high latitudes ion drag leads to the wind velocities considerably differing from the simple sub-solar to anti-solar flow. The strong zonal winds in the polar thermosphere (above 200 km) in Figure 4 are driven primarily by ion drag due to the high latitude convective electric fields (see also Section 4.3). In the low and mid latitude thermosphere the wind flow is primarily diurnal above around 200 km altitude and semidiurnal in the lower thermosphere.

One important process in the upper mesosphere (60-90 km) region that is not captured by GCMs driven by solar heating alone is the dissipation or breaking of atmospheric gravity waves which deposits momentum in that region. The wave drag gives rise to the closure and reversal of the zonal jets shown in Figure 4, a feature observed in the atmosphere which cannot be reproduced by models without including the gravity wave drag term in the momentum equation (Geller, 1983).

Internal gravity waves propagate vertically and may be driven either thermally, by surface topography, convection or shear instabilities in the background wind flow. Most families of gravity waves have horizontal phase speeds, c, of up to tens of meters per second with respect to the surface, but their vertical propagation is determined rather by the phase speed with respect to the mean flow, $\overline{u}$, in the atmosphere. As long as $\overline{u} - c \neq 0$ the waves do not interact with the background atmosphere. In the absence of any dissipation of the waves their amplitudes grow vertically as $\rho^{-1/2}$, with ρ being the mean atmospheric density, so amplitudes increase substantially with altitude. When $\overline{u} - c \approx 0$ the mean flow absorbs the wave and thereby acts as a barrier, preventing further vertical propagation. This and other dissipation mechanisms such as eddy and molecular diffusion or viscosity prevent further wave amplitude growth, filtering the wave spectrum and leading to deposition of horizontal momentum in the region of breaking or dissipation. Waves therefore act as an effective means of vertical coupling in the atmosphere, whereby horizontal momentum is transported vertically. The consequences of gravity wave dissipation and breaking are three-fold, they affect the zonal and meridional wind flow, lead to potentially significant turbulent mixing which affects the composition and thirdly they affect the thermal structure via primarily adiabatic heating and cooling. A comprehensive review of wave coupling on the terrestrial planets is given by Forbes (2002).

The gravity waves transporting most of the momentum in the Earth's atmosphere have horizontal wavelengths from 10's to 100's of km and are hence not resolved by global models. Gravity wave momentum deposition therefore needs to me included in these models in parameterized form. The gravity wave parameterization scheme used in CMAT is a hybrid Matsuno-Lindzen scheme (Meyer, 1999), one of several

available in the literature. The Lindzen scheme (Lindzen, 1981) assumes that amplitudes of gravity waves propagating vertically grow exponentially with height until a critical altitude is reached where wave perturbations create super-adiabatic lapse rates and the wave begins to break. The scheme gives an expression for eddy diffusion that translates into an expression of horizontal momentum that prevents the further growth of the wave above the critical level. Many alternative gravity wave drag parameterizations have been developed since, most recently by Medvedev and Klaassen (2000), and are used in General Circulation Models to better represent the middle atmosphere dynamics, although none of the schemes work for all scenarios. The TIME-GCM also includes gravity wave schemes which are adapted to the particular modeled scenarios to best match observations (Zhou et al., 1997). Gravity wave parameterizations can be regarded almost as a free parameter which is adjusted for resulting dynamics to best fit observations.

4.2 Dynamics on other planets and moons

No direct measurements have been made to-date of mesosphere/thermosphere winds in any planetary atmosphere except Earth. The techniques used to directly measure winds by remote sensing rely either on Doppler-shift determinations of emission spectra or time-tracking of distinct features such as clouds. Another technique used on Venus and most recently on Titan is that of tracking atmospheric probes as they descend through the atmosphere. None of these techniques however work in the upper cloud-free regions of atmospheres due to the low densities which hardly affect the motion of atmospheric probes there and make detection of Doppler shifts in atmospheric emissions challenging.

The planetary atmosphere currently best known apart from Earth is Venus, largely due to the Pioneer Venus mission which was in orbit from 1978 to 1992 and included 4 atmospheric probes which were dropped into the atmosphere early in the mission. One striking feature of Venus' atmosphere between the surface and the upper cloud top (around 70 km) is its super-rotation (Schubert, 1983; Gierasch et al., 1997) characterized by retrograde zonal winds reaching average velocities of $\sim$100 m/s over the equator. Several theories have been proposed to explain this, in particular meridional transport of momentum from mid-latitudes as a result of eddy mixing (Gierasch, 1975) and momentum pumping by thermal tides (Fels and Lindzen, 1974). Dynamics near the cloud top have been described as being the combination of a mean zonal super-rotating flow and two time-dependent features with each an amplitude of around 10 m/s, the solar tide and a 4-day traveling wave (Gierasch et al., 1997). Theoretical calculations of dynamics in Venus' thermosphere have predicted the presence of a strong sub-solar to anti-solar (SS-AS) flow driven by the large day-night temperature difference in the thermosphere (see Section 2) as well as a super-imposed time-varying retrograde super-rotating flow (Bougher et al., 1997). This circulation pattern has been indirectly confirmed by ground-based and spacecraft observations of nightside emissions at 1.27μm. These emissions result from

recombination of atomic oxygen atoms generated on the dayside from CO_2 photolysis and are associated with regions of downwelling in the atmosphere. Other emissions used as tracers include UV emissions in the NO γ and δ bands which result from the recombination of N and O. The reviews by Lellouch et al. (1997), Bougher et al. (1997; 2006a) and Schubert et al. (2007) give a comprehensive summary of emissions in Venus' atmosphere and their role in deriving wind speeds at different altitudes.

Waves, like on Earth, are thought to play a key role in the atmosphere of Venus. An early example of observed solar thermal tides was obtained from measurements by the Orbiter IR Radiometer (OIR) on board Pioneer Venus (Schofield and Taylor, 1983) which identified semidiurnal temperature oscillations peaking near 95 km altitude that are replaced at higher altitudes by diurnal changes due to thermospheric heating. In situ thermospheric gas density observations by the Pioneer Venus Orbiter Neutral Mass Spectrometer (PV-ONMS) revealed the presence of waves of horizontal scales ranging from 100-600 km (Kasprzak, et al., 1988) which have been interpreted as signatures of gravity waves propagating upward from the upper meso-

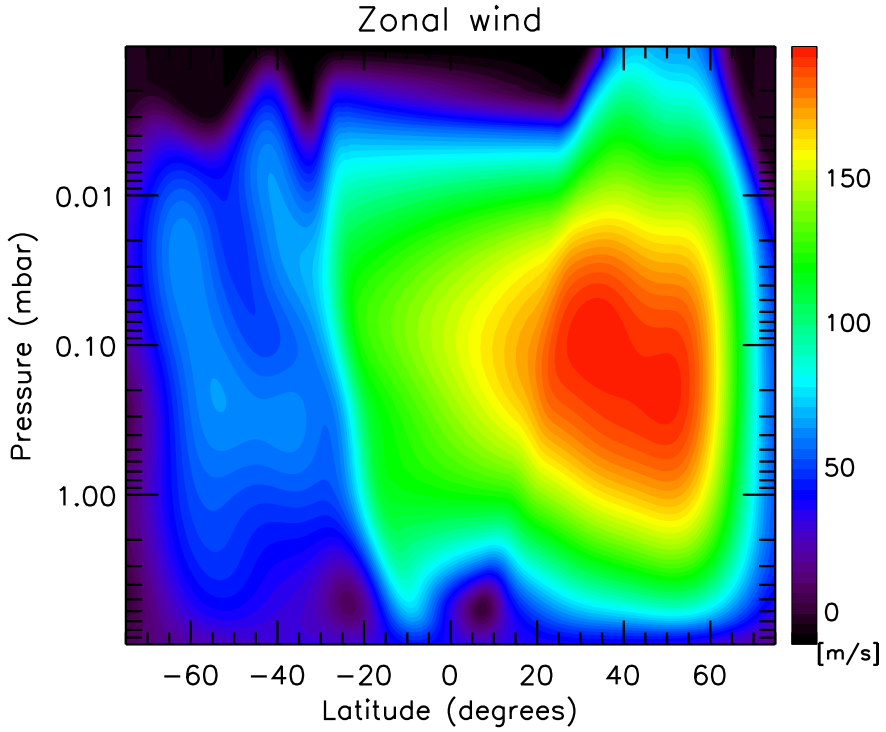

Fig. 5 Zonal winds (positive eastward) in Titan's stratosphere, as inferred from temperature observations by the Cassini Composite Infrared Spectrometer (CIRS) by Achterberg et al.(2008).

sphere region (Mayr et al., 1988) and depositing momentum into the background atmosphere at thermospheric altitudes, possibly supporting a super-rotating flow (Alexander, 1992). To-date, theoretical calculations of the Venus thermosphere cannot reproduce the large day-night temperature gradient (Section 2) without imposing an empirical drag term which slows down the sub-solar to anti-solar flow (Bougher et al., 2006a). Without this term, dynamics via adiabatic heating on the nightside reduce the day-night temperature difference to considerably smaller than observed values. It is possible that this drag is also a result of dissipating or breaking gravity waves, but further observations are needed to confirm this. Gravity wave drag parameterizations developed for Earth (see Section 4.1) are increasingly adapted to other planets like Venus, but remain "trial-and-error" approaches due to lack of sufficient observations to characterize the gravity wave spectra there (Bougher et al., 1997). The important role that gravity waves play for dynamics on Venus therefore pose a serious challenge to theoretical modelers. Observations by the ongoing Venus Express mission may help better constrain the dynamics on Venus and improve our understanding of the key momentum sources.

The other slowly rotating body with a substantial atmosphere is Titan. There, like on Venus, super-rotation has been detected in the stratosphere (Hubbard et al., 1993; Flasar et al., 2005b; Sicardy et al., 2006) with prograde wind velocities of around 100 m/s. Theories about the origin have been proposed which are essentially similar to those for Venus, and numerical simulations of Titan's stratospheric circulation have in part succeeded in reproducing the super-rotation without the need to artificially introduce further momentum sources (Hourdin et al., 1995). Measurements of the Doppler shift of the radio signals from the Huygens Probe gave in situ measurements of zonal wind on Titan near 10^0S latitude between the surface (1.5 bar) and 140 km altitude (3 mbar) (Bird et al. 2005). Recent observations by the Cassini Composite Infrared Spectrometer (CIRS) have helped construct temperature maps of Titan's stratosphere up to around 500 km altitude, allowing the derivation of zonal wind profiles using the thermal wind equation (Flasar et al., 2005b; Achterberg et al., 2008). Figure 5 shows that a strong eastward jet dominates the stratosphere on Titan. The current southern hemisphere summer conditions generate a hemispherically asymmetric profile. No direct measurements are available for higher altitudes on Titan, but calculations by Mueller-Wodarg et al. (2000; 2003; 2008) and Bell (2008) have shown that thermally driven winds could reach velocities in the order of 50-100 m/s in the thermosphere. One important factor in this was vertical coupling to the lower altitudes. Cassini observations in Titan's mesosphere (500-1000 km) region are too scarce to constrain dynamics, so little is known of winds at 1000 km, the bottom boundary of the region systematically examined by the Ion Neutral Mass Spectrometer (INMS). Further observations from Cassini during the extended mission will help further constrain dynamics on Titan and assess the role of waves identified in the Cassini and Huygens data (Fulchignoni et al., 2005; Mueller-Wodarg et al., 2006b).

No in situ wind measurements are presently available for the Mars upper atmosphere. Few ground-based observations were made to-date, focusing mostly on the middle atmosphere ($\sim$50-100 km) (Lellouch et al., 1991). Due to their scarcity

and coarse resolution, these measurements did not allow characterization of short term and seasonal trends in Martian winds. Most of our current knowledge of dynamics on Mars is derived from density, temperature, and nightglow observations from spacecraft and the inferred winds that result from the application of General Circulation Models to interpret these observations (Keating et al., 1998; Bougher et al., 1999, 2000, 2006b; Withers et al., 2003). One example of nightglow measurements on Mars are the hydrogen Lyman α (121.6 nm) and NO γ and δ band emissions (190-270 nm) observed in the winter polar night (Bertaux et al., 2005). These emissions, like those on Venus, are thought to be a result of dayside production of N and O atoms which are transported to the nightside by horizontal winds and to lower altitudes by subsiding winds, where they radiatively recombine to produce the NO nightglow. Density measurements such as those obtained from the Mars Global Surveyor Accelerometer readings (Keating et al, 1998) have shown the presence of features which have been interpreted as nonmigrating tides, one of many families of waves found to be present in the Mars upper atmosphere (Forbes and Hagan, 2000; Forbes et al., 2002; 2004; Forbes, 2002). While dynamics in the upper atmosphere are thought to be driven primarily by solar EUV heating, studies have suggested that vertical dynamical coupling nevertheless plays an equally significant role on Mars as it does on Venus and Earth, most prominently in the form of strong wave signatures in the thermosphere that are not only formed in situ at those altitudes, but also include effects due to topography (Forbes et al., 2002). Bougher et al. (2006b) and Bell et al. (2007) additionally proposed the existence of a deep inter-hemispheric circulation in order to enable thermospheric winter polar warming to operate. While most models available to-date still rely on implementing this coupling to lower altitudes as a lower boundary condition (Bougher at al., 2008), codes are now appearing for Mars with a vertical range from the ground to the thermosphere (González-Galindo et al., 2005), having the advantage of more self-consistently including processes of vertical dynamical coupling.

Winds on the Gas Giants are dominated by the fast rotation periods of the solid planets (Table 1) which gives rise to primarily geostrophic circulation due to the large Coriolis accelerations. The presence of strong zonal jets in the troposphere Saturn is well known (Flasar et al., 2004; Flasar et al., 2005a), with some evidence of their presence reaching into the stratosphere and mesosphere as well (Hubbard et al., 1997). Saturn's zonal winds are still not well understood. Wind speeds derived from cloud tracking indicated values of 500 m/s near the equator (Ingersoll et al., 1984; Barnet et al., 1992) which would imply a considerable excess of axial angular momentum present in the atmosphere relative to Saturn's interior. Cloud tracking observations made more recently (1996-2002) with the Hubble Space Telescope (HST) suggest smaller equatorial winds of up to 275 m/s (Sánchez-Lavega et al., 2003), values largely confirmed by the latest Cassini-CIRS observations (Flasar et al., 2005a). The discrepancy between earlier and more recent observations is currently not well understood, and it is unclear whether the difference represents a real change in the atmosphere or an observational uncertainty. No observational evidence is available for winds in Saturn's mesosphere and thermosphere, but calculations by Mueller-Wodarg et al. (2006a) demonstrated the likely dominance of

zonal flow there as well. Little is known also about stratospheric and (especially) tropospheric winds on Jupiter. In situ measurement were obtained with a Doppler wind profiler on the Galileo Probe (Atkinson et al., 1996), but the probe sampled an anomalous, cloud-free location (Orton et al., 1996), so the winds it measured may not be representative for Jupiter. As for Saturn, all other wind measurements on Jupiter have been indirect and based on simplifying assumptions such as a non-scattering atmosphere (in the temperature retrievals) and the gradient wind balance (Flasar et al., 2004). General circulation models for the upper atmospheres of Jupiter and Saturn (Achilleos et al., 1998; Bougher et al., 2005; Mueller-Wodarg et al., 2006) have helped predict what dynamics in the thermosphere and ionosphere could be, but many aspects of these calculations still await validation by observations. One particular uncertainty is the source of unexpectedly high temperatures in the thermospheres of all Gas Giants (see Section 2), which will affect not only the thermal structure but also the global dynamics. Upward propagating waves, one possible candidate energy source (Yelle and Miller, 2004), may also deposit significant amounts of momentum in the upper atmospheres. One additional source of momentum in the thermospheres of Earth, Jupiter and Saturn is ion drag, discussed in the following. In the auroral regions additional thermal energy sources are Joule heating and particle precipitation, which via temperature and pressure gradients further alter the dynamics.

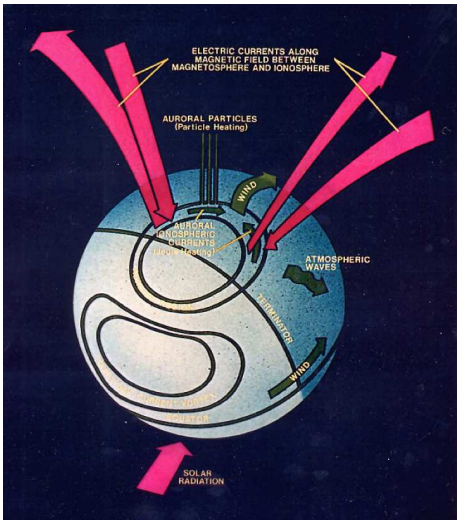

Fig. 6 Schematic of the auroral particle and joule heat inputs and current systems in the Earth's polar upper atmosphere (Roble, 1996).

4.3 Auroral dynamics

It is well known that both solar EUV radiation and auroral energy and momentum sources have a significant effect on the Earth's thermospheric and ionospheric structure and dynamics. A schematic of the auroral particle and joule heat inputs and current systems is shown in Fig. 6.

Upper atmosphere general circulation models using these forcings (Roble et al., 1988; Fuller-Rowell et al., 1996) have been reasonably successful in simulating the thermosphere and ionosphere responses for a wide range of auroral activity. Figure 7 is a schematic of the zonally averaged mass flow stream function illustrating the response of the circulation to increasing levels of auroral activity. The aurora increases from geomagnetic quiet conditions with an energy input of 10^{10} W to geomagnetic moderate conditions with an energy input of 10^{11} W to a geomagnetic storm with and energy input of 10^{12} W. During equinox when the sun is directly over the equator, the circulation is from the equator toward the poles in both hemispheres. Auroral energy input occurs at high magnetic conjugate latitudes in both hemispheres and the increased heating drives a circulation cell from high latitudes toward the equator. As geomagnetic activity increases the auroral equatorward circulation intensifies, forcing the reversal of the solar directed poleward flow and the equatorward directed auroral flow to move equatorward and to lower altitudes as shown in the left panels.

For solstice there is a similar situation. The December solstice solar circulation is from the summer pole in the southern hemisphere to the winter pole in the northern

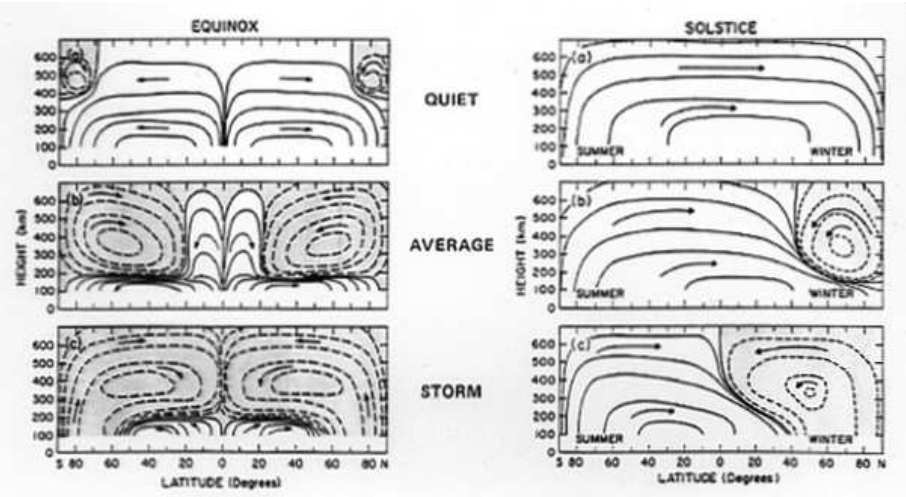

Fig. 7 Zonally averaged mass flow stream function illustrating the circulation in the Earth's upper atmosphere for equinox (left) and southern hemisphere summer (right) conditions at quiet, average and strong levels of geomagnetic activity. (Roble et al., 1983)

hemisphere. In the summer hemisphere the joule and auroral heating reinforces the summer-to-winter circulation whereas in the winter hemisphere, joule and auroral heating is sufficiently strong to produce a small equatorward flow at high latitudes during geomanetic quiet conditions. For moderate conditions the circulations are enhanced and for geomagnetic storms both the solar driven summer hemisphere and winter reverse cells are both enhanced. With geomagnetic activity being highly variable, the pattern varies between the quiet, moderate and storm conditions. These schematics represent the zonal mean circulation or mean flow. During impulsive events the auroral heat and momentum source can launch large scale thermospheric waves that can travel equatorward at speeds of up to 700 m/s at F-region altitudes near 300 km and waves in the lower thermosphere near 150 km of 300-400 m/s. Thus, the thermospheric response is a complex mixture of the overturning of the mean circulation with various impulsive waves superimposed.

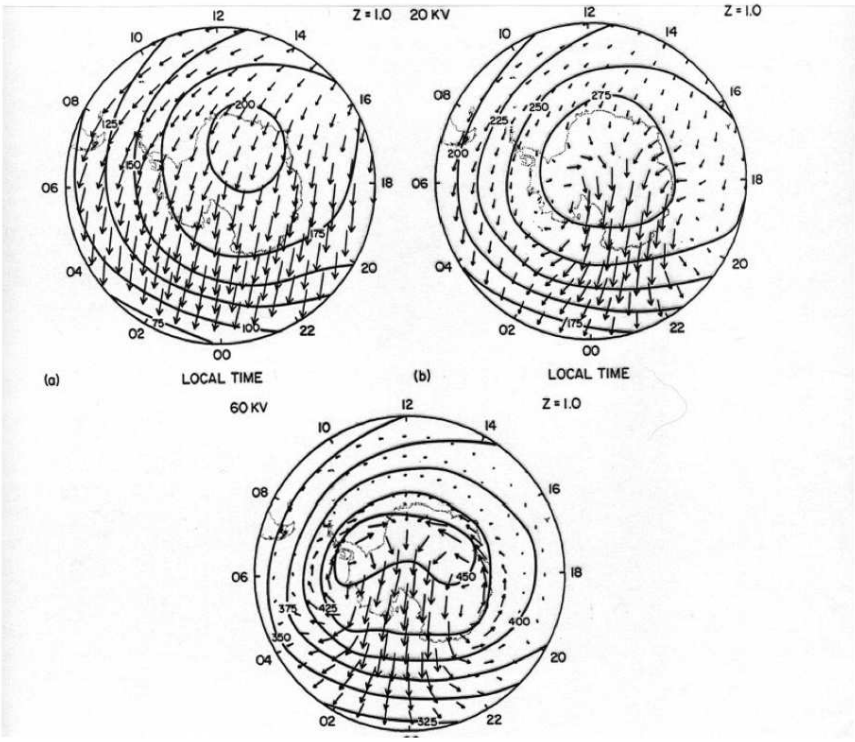

Fig. 8 Schematic showing the response of the high latitude thermosphere to different levels of auroral forcing. Contour lines are exospheric temperatures, arrows are neutral winds. The upper left panel shows the solar-driven situation only, the upper right panel shows a situation with quiet geomagnetic conditions (cross-cap potential 20 kV) and the bottom panel is for moderate geomagnetic conditions (cross-cap potential 60 kV).

Figure 8 (Roble et al., 1983) is a schematic showing the response of the high latitude thermosphere to different levels of auroral forcing. The top left panel shows a TGCM calculation of perturbation temperature (from a global mean) for a case where the circulation is due to solar heating alone, without auroral particle precipitation or joule heating. Here, the flow is from the dayside to the nightside, essentially perpendicular to isobars, with some influence of Coriolis forces. The top right panel shows the perturbation temperature and circulation for the case of geomagnetic quiet conditions with only a 20 kV cross polar cap potential drop driving ion convection and the lower panel is for moderate steady state forcing of 60 kV cross polar cap. The interaction of the solar wind with the earth's geomagnetic field produces a dawn-to-dusk potential drop and the corresponding ExB drift generates a two cell pattern in the ion drift that transfers momentum to the neutral gas which tends to follow the ion convection pattern. The principle can be compared to a giant "egg beater" operating over the high latitude thermoshere. In addition to the ion drag momentum source, auroral Joule and particle heating occur along the convecting ion boundaries in an oval in the lower thermosphere. Thus, the aurora heats the thermosphere 100-500 K and generates winds approaching 200-600 m/s at 300 km. Again, the pattern is highly variable because of the variability in the aurora.

With Jupiter and Saturn having internal magnetic fields as well of sufficient strength to produce gyrofrequencies smaller than ion-neutral collision frequencies in the ionospheres near the peak density heights, similar dynamical coupling is expected to occur there as well. No direct neutral wind observations exist in the au-

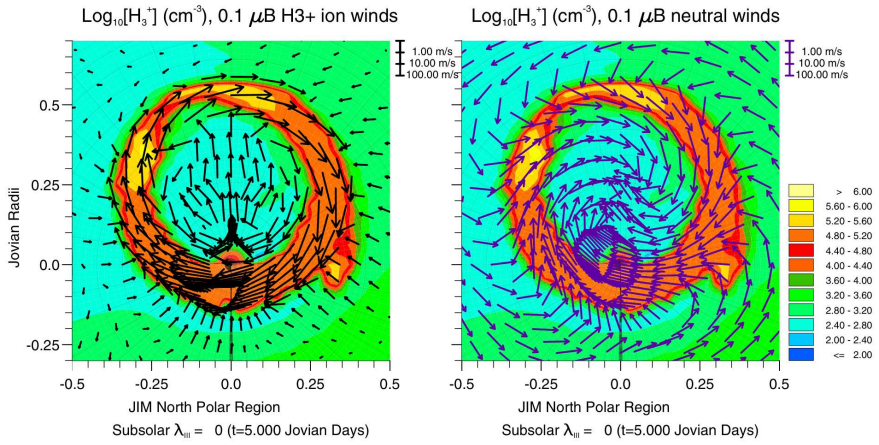

Fig. 9 Global model profiles of ionization and velocity in the co-rotating frame for the northern polar region of Jupiter. Left panel: Colour contours of H_3^+ density over a 0.1 μbar pressure surface (location of the auroral ion peak). Arrows represent the horizontal ion velocities, following the mixed linear/log velocity scale bar shown. The meridian (vertically downward in plot) indicates the zero longitude and subsolar point. Right panel: As for the left panel, but with arrows now representing the neutral horizontal wind velocity. From Achilleos et al. (2001)

roral regions of Jupiter or Saturn, but ground-based observations of Doppler shifts in the H_3^+ $\nu 2$ $Q(1,0^-)$ line at 3.953 μm have detected westward ion velocities in the auroral regions of Jupiter reaching 1.5 km/s (Stallard et al., 2001). Similar observations for Saturn detected H_3^+ westward velocities implying the auroral region was sub-corotating by up to a factor of 0.43 (Stallard et al., 2007). Simulations with the General Circulation Model of Jupiter by Achilleos et al., (1998; 2001) have shown that ion velocities driven by convection electric fields in the auroral regions can through ion-neutral collisions drive neutral wind velocities of around half the ion speeds (Figure 9). To-date, accurate models of the convection electric field on Jupiter are not available, so most of these simulations rely on simplified electric field models adapted from Earth conditions which do not reflect the high time variability of the real auroral regions. It is likely that the factor of momentum transfer from the ions to the neutrals is nevertheless accurate within an order of magnitude, implying significant influence of the ion velocities on thermospheric winds, as on Earth. Similar results were found by calculations of Bougher et al., (2005) using their JTGCM code of Jupiter's thermosphere and ionosphere, for which ion velocities (up to 1.5 to 3.0 km/sec) drove neutral velocities up to 1.0 to 1.2 km/sec.

5 Key outstanding problems and future needs

As the result of highly sophisticated and successful space missions, Earth based observations and theoretical models, the past decades have seen major advances in our understanding of the atmospheres of Earth and other planets or moons, in particular Venus and Titan, followed by Jupiter, Mars and Saturn. Little is known yet about Uranus and Neptune as well as Triton and Pluto. The New Horizons mission will help considerably in advancing our knowledge about Pluto's atmosphere after its scheduled arrival in 2015, providing the first ever close-up view of Pluto and Charon, which have never been visited by any spacecraft. Several future missions to the outer solar system are currently in planning or under study, including the Juno mission to Jupiter which is due for launch in 2011 and either a Jupiter/Europa mission or Titan/Enceladus mission. The next planned mission to Venus is Planet-C, lead by the Japanese Space Agency (Jaxa) and is due for launch in summer of 2010. Future planned missions to Mars include Nasa's Mars Science Laboratory (launch in Fall 2009), Nasa's Mars Scout mission (launch in or after 2013) and ESA's Aurora Flagship mission currently named Exomars which is due for launch in 2011 or later.

Despite the significant advances over the past decades, a large number of scientific questions remain open about the aeronomy of many planets in our solar system, including our own. Our knowledge has now advanced enough about most atmospheres that we begin to obtain a first understanding of aeronomic processes under different conditions and can ask increasingly sophisticated questions. The following outlines only a few of these scientific questions.

5.1 Energy crisis on Giant Planets

As outlined in Section 2 we currently do not understand the thermal balance on Gas Giants. With solar EUV heating and magnetospheric energy sources being insufficient to explain observed thermospheric temperatures outside the auroral regions, the most likely candidate sources for the energy are the interiors of the planets. Energy can be transferred to the outer regions of the atmospheres via propagating waves, but the only in situ observations available to-date for Jupiter by the Galileo probe (Seiff et al., 1997) did not resolve this issue. The observed gravity waves could not unambiguously be shown to be able to transport the required amount of energy into Jupiter's thermosphere (Yelle and Miller, 2004). A more substantial programme of observation is needed to resolve this issue, one of the key aeronomy problems to-date. Atmosphere probes such as the Galileo probe may considerably help in answering this question.

5.2 Dynamics in planetary atmospheres

Despite the plentiful availability of atmospheric wind profiles obtained through remote sensing for most planets, aeronomy studies suffer from a severe shortage of direct wind measurements. Only on Earth have upper atmosphere winds been sampled directly, with some direct measurements in the lower atmospheres available for Venus and Titan. Mostly, winds are inferred from thermal profiles by applying either simple approximations (thermal wind equation, geostrophic approximation) to derive winds from horizontal or vertical thermal gradients or "tuning" General Circulation Models to reproduce the thermal structure and obtain the necessary global dynamic structure from those. Another method commonly used is observation of doppler shifts in atmospheric gas emissions, but those are restricted to regions of significant (detectable) atmospheric gas emissions, which is usually below the thermosphere only. As a result of limited vertical coverage of wind measurements we still have an incomplete understanding of the global circulation system on most planets. For all planets we are in need for more direct and more comprehensive measurements of winds throughout the atmosphere, either by tracking balloons or more systematically observing emissions from the upper atmospheres.

5.3 Stratospheric constituents on the giant planets

Systematic measurements are needed of the latitude, altitude, and time variation of stratospheric constituents on the giant planets. This information is necessary to help constrain heating rates and circulation. The stratospheric energy balance is largely determined from absorption of solar radiation and the re-emission of this energy and radiative transfer it undergoes. Understanding these problems requires a detailed in-

ventory of stratospheric constituents and, importantly, their horizontal and vertical distribution. Not only is their distribution important for understanding the heating rates, but some of the more inert gases can also be seen as tracers for atmospheric dynamics. Understanding their latitudinal and seasonal distribution will considerably help us understand the dynamics and chemistry of Gas Giants.

5.4 Atmospheric waves

As shown in section 4 atmospheric waves on all scales play a key role in vertical coupling within an atmosphere. Studies of the Earth's atmosphere have shown that we cannot understand the global dynamics without considering the effects of gravity wave drag. In the thermosphere the diurnal tide leads to removal of O via an enhancement in the effective recombination rate due to vertical (downward) transport by the tide. The problem of gravity waves on Earth is still not fully understood and often taken as a degree of freedom. "Tuning" the gravity wave drag parameterization often allows theoreticians to fit their calculations to observations, but this approach ultimately remains unsatisfying. On other planets the wave spectra are even less known and will probably never be fully understood, but as systematic programme of observation of larger-scale atmospheric waves would be of considerable benefit. This can best be achieved by orbiting spacecraft which dedicate part of their observations to monitoring of the atmosphere and its periodic fluctuations.

5.5 Heating efficiencies and CO_2(v2)-O relaxation rates

The thermal balance on planets Venus, Earth and Mars critically relies on IR cooling by the CO_2 molecule, mostly at 15 μm, which is considerably affected by vibrational excitation of CO_2 by O (Section 2). The CO_2(v2)-O relaxation rate however is still poorly known, allowing considerable degrees of freedom in our understanding of the thermal balance on these planets. Systematically carrying out experiments such as recent simultaneous observation of the responses of Venus, Earth and Mars to changes in solar flux (Forbes et al., 2006) may help resolve this problem, but additionally laboratory measurements need to be carried out to constrain this rate. Laboratory experiments are also needed to measure the heating efficiencies of CO_2. As discussed by Fox (1998), theoretical models rely on lower heating efficiencies than can be justified from molecular calculations in order to reproduce observed thermospheric temperatures. This shortcoming highlights another uncertainty in our understanding of the thermal balance on terrestrial planets. Our current knowledge of the CO_2(v2)-O relaxation rates is discussed by Huestis et al. (2008).

5.6 Atomic oxygen on Mars

No direct measurements exist to-date of atomic oxygen on Mars. This constituent is not only an important tracer of dynamics, but plays a key role in the thermal balance of the thermosphere and photochemistry of the ionosphere. This therefore constitutes a major unknown for our understanding of aeronomy on Mars.

Acknowledgements IMW is funded through a University Research Fellowship by the Royal Society London. JM gratefully acknowledges support from the NASA Planetary Atmospheres program grant NNX08AF05G. SWB acknowledges NASA grant NNX07A084G that supported research and writing for this chapter.

Table 1 Main properties of non-transient atmospheres in the solar system

Object	Mean heliocentric distance	Duration of mean solar day	Principal gases	Surface or 1 bar level P, T	Exobase height	Dayside exosphere temperature
Venus	0.72 AU	116.75 days[a]	CO_2, N_2, SO_2, O	92 bar, 735 K	160 km	230-325 K
Earth	1.00 AU	1 day	N_2, O_2, O	1 bar, 185-331 K	450 km	600-2000 K[c]
Mars	1.52 AU	1.03 days	CO_2, N_2, O	6 mbar, 140-270 K	180 km	180-325 K
Jupiter	5.20 AU	$9^h55^m27^s$	H_2, He, H, CH_4	1 bar, 165 K	1600 km[b]	940 K[c]
Saturn	9.54 AU	$10^h39^m22^s$	H_2, He, H, CH_4	1 bar, 160 K	2500 km[b]	420 K[c]
Titan	9.54 AU	15.95 days	N_2, CH_4, H	1.4 bar, 94 K	1430 km	150 K
Uranus	19.19 AU	$17^h14^m24^s$	H_2, He, H, CH_4	1 bar, 76 K	4700 km[b]	670 K[c]
Neptune	30.07 AU	$16^h6^m36^s$	H_2, He, H, CH_4	1 bar, 73 K	2200 km[b]	470 K[c]
Triton	30.07 AU	5.88 days[a]	N_2, CO, CH_4, H_2	14 μbar, 38 K	930 km	100 K
Pluto	39.48 AU	6.39 days[a]	N_2, CO, CH_4, H_2	3-90 μbar, 35-50 K	1800 km	100 K

[a] Retrograde rotation [b] Above the 1 bar level [c] In the non-auroral regions

References

1. A'Hearn, M. F. , R.L. Millis, D.G. Schleicher, D.J. Osip, P.V. Birch, Icarus 118, 223270 (1995)
2. Achilleos, N., S. Miller, J. Tennyson, A. D. Aylward, I. C. F. Mueller-Wodarg, and D. Rees (1998), JIM: A time-dependent, three-dimensional model of Jupiter's thermosphere and ionosphere, J. Geophys. Res. **103**, 20089-20112.
3. Achilleos, N., S. Miller, R. Prangé, G. Millward, and M. K. Dougherty (2001), A dynamical model of Jupiter's auroral electrojet, New J. of Physics **3**, 3.1-3.20.
4. Achterberg, R. K., B. J. Conrath, P. J. Gierasch, F. M. Flasar and C. A. Nixon (2008), Titan's Middle-Atmospheric Temperatures and Dynamics Observed by the Cassini Composite Infrared Spectrometer, Icarus, in press, 2008.
5. A'Hearn, M. F., R. L. Millis, D. G. Schleicher, D. J. Osip, P. V. Birch (1995), The ensemble properties of comets: Results from narrowband photometry of 85 comets, 1976-1992, Icarus **118**, 223-270.
6. Alexander, M. J. (1992), A mechanism for the Venus thermospheric superrotation, Geophys. Res. Lett. **19**, 2207-2210.
7. Atkinson, D. M., J. B. Pollack, and A. Seiff (1996), Galileo Doppler measurements of the deep zonal winds at Jupiter. Science **272**, 842-843.
8. Atreya, S.K. et al. (1999), A comparison of the atmospheres of Jupiter and Saturn: deep atmospheric composition, cloud structure, vertical mixing, and origin, Planet. Space Sci., **47**, 1243-1262.
9. Atreya, S. K., and Z. G. Gu (1994). Stability of the Martian atmosphere: Is heterogeneous catalysis essential? J. Geophys. Res. **99**, 13133-13145.
10. Atreya, S. K. , P. R. Mahaffy, H. B. Niemann, M. H. Wong and T. C. Owen (2002), Composition and origin of the atmosphere of Jupiteran update, and implications for the extrasolar giant planets, Planet. Sp. Sci., **51**, 105-112, doi:10.1016/S0032-0633(02)00144-7
11. Atreya, S. K., E. Y. Adama, H. B. Niemann, J. E. Demick-Montelara, T. C. Owen, M. Fulchignoni, F. Ferri, and E. H. Wilson (2006). Planet. Space Sci. **54**, 1177-1187.
12. Atreya, S. K., P. R. Mahaffy, and A.-S. Wong (2007). Methane and related trace species on Mars: Origin, loss, implications for life, and habitibility. Planet. Space Sci. **55**, 358-369.
13. Banaszkiewicz, M., L. M. Lara, R. Rodrigo, J. J. López-Moreno, and G. J. Molina-Cuberos (2000). A coupled model of Titan's atmosphere and ionosphere. Icarus **147**, 386-404.

14. Bar-Nun, A., and V. Dimitrov (2006). Methane on Mars: A product of H_2O photolysis in the presence of CO. Icarus **181**, 320-322.
15. Barnet, C. D., J. A. Westphal, R. F. Beebe, and L. F. Huber (1992), Icarus **100**, 499.
16. Bell, J. M., S. W. Bougher, and J. R. Murphy (2007), Vertical dust mixing and the interannual variations in the Mars thermosphere, J. Geophys. Res., **112**, E12002, doi:10.1029/2006JE002856.
17. Bell, J. M., (2008), The Dynamics of the Upper Atmospheres of Mars and Titan, U. of Michigan, Ph.D. Thesis.
18. Bergin, E. A., et al. (2000). Submillimeter Wave Astronomy Satellite observations of Jupiter and Saturn: Detection of 557 GHz water emission from the upper atmosphere. Astrophys. J. **539**, L147-L150.
19. Bertaux, J. L., et al. (2005), Nightglow in the Upper Atmosphere of Mars and Implications for Atmospheric Transport, Science **307**, 566-569, doi:10.1126/science.1106957.
20. Bertaux, J. - L., et al. (2007), A warm layer in Venus' cryosphere and high-altitude measurements of HF, HCl, H_2O and HDO, Nature, **450**, doi:10.1038/nature05974.
21. Bézard, B., and D. Gautier (1985). A seasonal climate model of the atmospheres of the giant planets at the Voyager encounter time. I. Saturn's stratosphere. Icarus **61**, 296-310.
22. Bézard, B., E. Lellouch, D. Strobel, J.-P. Maillard, and P. Drossart (2002). Carbon monoxide on Jupiter: Evidence for both internal and external sources. Icarus **159**, 95-111.
23. Bird, M. K., et al. (2005), The vertical profile of winds on Titan, Nature **438**, 800-802, doi:10.1038/nature04060.
24. Bishop, J., P. N. Romani, and S. K. Atreya (1998). Voyager 2 ultraviolet spectrometer solar occultations at Neptune: Constraints on the abundance of methane in the stratosphere. J. Geophys. Res. **97**, 11681-11694.
25. Biver, N., D. Bockelée-Morvan and J. Crovisier, et al. (2002), Chemical composition diversity among 24 comets observed at radio wavelengths, Earth Moon Planets **90**, 323-333.
26. Bockelée-Morvan, D. and J. Crovisier (1987), The role of water in the thermal balance of the coma, ESA SP-278, 235-240.
27. Bockelée-Morvan, D., J. Crovisier, M. J. Mumma, H. A. Weaver (2005), The composition of cometary volatiles, in: *Comets II*, ed. by M. C. Festou, H. U. Keller, H. A. Weaver, Univ. Arizona Press, Tucson, 391-423.
28. Boggard et al. (2001), Martian volatiles: Isotopic composition, origin, and evolution, Chronology and Evolution of Mars, **96**, 425-458
29. Boissier, J., D. Bockelée-Morvan, N. Biver, et al. (2007), Interferometric imaging of the sulfur-bearing molecules H_2S, SO and CS in comet C/1995 O1 (Hale-Bopp), Astron. Astrophys. **475**, 1131-1144.
30. Bougher, S. W., D. M. Hunten, and R. G. Roble (1994), CO_2 cooling in terrestrial planet thermospheres, J. Geophys. Res. **99**, 14609-14622.
31. Bougher, S. W. , M. J. Alexander and H. G. Mayr (1997), Upper atmosphere dynamics: global circulation and gravity waves. In: S. W. Bougher, D. M. Hunten and R. J Phillips, Editors, Venus II, University of Arizona Press, Tucson, 259-291.
32. Bougher, S. W., S. Engel, R. G. Roble, and B. Foster (1999), Comparative terrestrial planet thermospheres: 2. Solar cycle variation of global structure and winds at equinox, J. Geophys. Res. **104**, 16591-16611.
33. Bougher, S. W., S. Engel, R. G. Roble, and B. Foster (2000), Comparative terrestrial planet thermospheres 3. Solar cycle variation of global structure and winds at solstices, J. Geophys. Res. **105**, 17,669-17,689.
34. Bougher, S. W., J. H. Waite Jr., T. Majeed, and G. R. Gladstone (2005), Jupiter Thermospheric General Circulation Model (JTGCM): Global structure and dynamics driven by auroral and Joule heating, J. Geophys. Res., **110**, E04008, doi:10.1029/2003JE002230.
35. Bougher, S. W., S. Rafkin, and P. Drossart (2006a), Dynamics of the Venus upper atmosphere: Outstanding problems and new constraints expected from Venus Express, Planet. Sp. Sci **54**, 1371-1380, doi: 10.1016/j.pss.2006.04.023.

36. Bougher, S. W., J. M. Bell, J. R. Murphy, M. A. López-Valverde, and P. G. Withers (2006b), Polar warming in the Mars thermosphere: Seasonal variations owing to changing insolation and dust distributions, Geophys. Res. Lett. **33**, L02203, doi:10.1029/2005GL024059.
37. Bougher, S. W., P.-L. Blelly, M. Combi, J. Fox, I. C. F. Mueller-Wodarg, A. Ridley, and R. G. Roble (2008), Neutral Upper Atmosphere and Ionosphere Modeling, *this volume*.
38. Brasseur, G. P., and S. Solomon (2005). *Aeronomy of the Middle Atmosphere*. Springer, Dordrecht.
39. Brasseur, G. P., J. J. Orlando, and G. S. Tyndall, Eds. (1999). *Atmospheric Chemistry and Global Change*. Oxford University Press, New York.
40. Brinton, H. C., H. A. Taylor, H. B. Niemann, H. G. Mayr, A. F. Nagy, T. E. Cravens, and D. F. Strobel (1980), Venus nighttime hydrogen bulge, Geophys. Res. Lett., **7**, 865-868.
41. Burgdorf, M., G. Orton, J. van Cleve, V. Meadows, and J. Houck (2006). Detection of new hydrocarbons in Uranus' atmosphere by infrared spectroscopy. Icarus **184**, 634-637.
42. Canaves, M. V., A.A. de Almeida, D.C. Boice, G.C. Snzovo (2007), On the chemistry of CS and NS in cometary comae, Adv. Space Res. **39**, 451-457.
43. Clancy, R. T., and H. Nair (1996). Annual (perihelion-aphelion) cycles in the photochemical behavior of the global Mars atmosphere. J. Geophys. Res. **101**, 12785-12790.
44. Cravens, T. E., et al. (2006). Composition of Titan's ionosphere. Geophys. Res. Lett. **33**, L07105, doi:10.1029/ 2005GL025575.
45. Crifo, J. F., M. Fulle; N. I. Kmle, K. Szego (2005), Lessons from physical models, in: *Comets II*, ed. by M. C. Festou, H. U. Keller, H. A. Weaver, Univ. Arizona Press, Tucson, 471-503.
46. Combi, M. R., W. M. Harris, W. H. Smyth (2005), Gas dynamics and kinetics in the cometary coma: Theory and observations, in: *Comets II*, ed. by M. C. Festou, H. U. Keller, H. A. Weaver, Univ. Arizona Press, Tucson, 523-552.
47. Combi, M. R., K. Kabin, D. De Zeeuw, T.I. Gombosi, K.G. Powell (1999), Dust-gas interrelations in Comets: Observations and theory, Earth Moon Planets **79**, 275-306.
48. Coustenis, A., A. Salama, E. Lellouch, T. Encrenaz, G. L. Bjoraker, R. E. Samuelson, T. de Graauw, H. Feuchtgruber, and M. F. Kessler (1998). Evidence for water vapor in Titan's atmosphere. Astron. Astrophys. **336**, L85-L89.
49. Crovisier, J. (1989), The photodissociation of water in cometary atmospheres, Astron. Astrophys. **213**, 459-464.
50. Crovisier, J. (1994), Photodestruction rates for cometary parent molecules, J. Geophys Res. Planets **99**, 3777-3781.
51. Crovisier, J. (2007), Cometary diversity and cometary families. Proceedings of the *XVIIIemes Rencontres de Blois: Planetary Science: Challenges and Discoveries*, astro-ph/0703785.
52. Dauphus, N. (2003), The dual origin of the terrestrial atmosphere, Icarus, **165**, 326-339.
53. De Bergh, C. et al. (2006), The composition of the atmosphere of Venus below 100 km altitude: An overview, Planet. Space Sci., **54**, 1389-1397.
54. Dello Russo, N., R. J. Vervack Jr , H. A. Weaver, et al. (2007), Compositional homogeneity in the fragmented comet 73P/Schwassmann-Wachmann 3, Nature **448**, 172-175.
55. DeMore, W. B., M. T. Leu, R. H. Smith, and Y. L. Yung (1985). Laboratory studies on the reactions between chlorine, sulfur dioxide, and oxygen: Implications for the Venus stratosphere. Icarus **63**, 247.
56. de Pater, I., H. Roe, J. R. Graham, D. F. Strobel, and P. Bernath (2002). Detection of forbidden SO $a^1\Delta$–$X^3\Sigma^-$ rovibronic transition on Io at 1.7 μm. Icarus **156**, 296-301.
57. de Pater, I., C. Laver, F. Marchis, H. G. Roe, and B. A. Macintosh (2007). Spatially resolved observations of the forbidden SO $a\Delta \rightarrow X\Sigma$ rovibronic transition on Io during an eclipse and a volcanic eruption at Ra Patera. Icarus **191**, 172-182.
58. Donahue, T. M. (1999), New Analysis of Hydrogen and Deuterium Escape from Venus, Icarus, **141**, 226-235.
59. Drossart, P., et al. (2007), A dynamic upper atmosphere of Venus as revealed by VIRTIS on Venus Express, Nature, **450**, doi:10.1038/nature06140.
60. Duncan, R. A. (1969), F-region seasonal and magnetic storm behaviour, J. Atmos. Terr. Phys., **31**, 59-70.

61. Elliot, J. L., D. F. Strobel, X. Zhu, J. A. Stansberry, L. H. Wasserman, and O. G. Franz (2000), The Thermal Structure of Triton's Middle Atmosphere, Icarus, **143**, 425-428.
62. Elliot, J. L., Person, M. J., Gulbis, A. A. S., et al. (2007), Changes in Pluto's atmosphere: 1988-2006. Astron. J. **134**, 1-13.
63. Encrenaz, T., B. Bézard, T. K. Greathouse, M. J. Richter, J. H. Lacy, S. K. Atreya, A. S. Wong, S. Lebonnois, F. Lefèvre, and F. Forget (2004). Hydrogen peroxide on Mars: evidence for spatial and seasonal variations. Icarus **170**, 424-429.
64. Fegley, B., Jr., and M. Yu. Zolotov 2000. Chemistry of sodium, potassium, and chlorine in volcanic gases on Io, Icarus **148**, 193-210.
65. Fels, S. B., Lindzen, R. S., 1974. The interaction of thermally excited gravity waves with mean flows. Geophys. Fluid Dyn. **6**, 149-191.
66. Feuchtgruber, H., E. Lellouch, T. de Graauw, B. Bézard, T. Encrenaz, and M. Griffin (1997). External supply of oxygen to the atmospheres of the giant planets, Nature **389**, 159-162.
67. Feuchtgruber, H., E. Lellouch, T. Encrenaz, B. Bézard, A. Coustenis, P. Drossart, A. Salama, T. de Graauw, and G. R. Davis (1999). Oxygen in the stratospheres of the giant planets and Titan. In The Universe as Seen by ISO, edited by P. Cox and M. F. Kessler, 133-136, ESA SP-427.
68. Finlayson-Pitts, B. J., and J. N. Pitts, Jr. (1999). Chemistry of the Upper and Lower Atmosphere. Academic Press, San Diego.
69. Flasar, F. M., et al. (2004), An intense stratospheric jet on Jupiter, Nature, **427**, 132-135.
70. Flasar, F. M., et al. (2005a). Temperatures, winds, and composition in the Saturn system. Science **307**, 1247-1251.
71. Flasar, F. M., et al. (2005b), Titan's atmospheric temperatures, winds, and composition, Science **308**, 975-978, doi:10.1126/science.1111150.
72. Forbes, J. M. (2002), Wave coupling in terrestrial planetary atmospheres, in: Mendillo, M., Nagy, A., Waite, J. H. (Eds.), Atmospheres in the Solar System: Comparative Aeronomy. Geophysical Monograph **130**, American Geophysical Union, Washington, DC, 171-190.
73. Forbes, J. M., and M. E. Hagan (2000), Diurnal Kelvin wave in the atmosphere of Mars: towards an understanding of stationary density structures observed by the MGS accelerometer, Geophys. Res. Lett. **27**, 3563-3566.
74. Forbes, J .M., A. F. C. Bridger, S. W. Bougher, M. E. Hagan, J. L. Hollingsworth, G. M. Keating, and J. Murphy (2002), Nonmigrating tides in the thermosphere of Mars, J. Geophys. Res. **107**, doi:10.1029/2001JE001582.
75. Forbes, J. M., X. Zhang, M. Angelats i Coll, and G. M. Keating (2004), Nonmigrating tides in the thermosphere of Mars: a quasi-empirical description, Adv. Sp. Res. **34**, 1690-1695.
76. Forbes, J. M., S. Bruinsma, and F. G. Lemoine (2006), Solar Rotation Effects on the Thermospheres of Mars and Earth, Science, **(**312), 1366-1368, doi:10.1126/science.1126389.
77. Formisano, V., S. K. Atreya, T. Encrenaz, N. Ignatiev, and M. Giuranna (2004). Detection of methane in the atmosphere of Mars. Science **306**, 1758-1761.
78. Fox, J. L. (1998), Heating efficiencies in the thermosphere of Venus reconsidered, Planet. Sp. Sci. **36**, 37-46.
79. Fox, J. L. (2004). Advances in the aeronomy of Venus and Mars. Adv. Space Res. **33**, 132-139.
80. Fox, J. L., and S. W. Bougher (1991). Structure, luminosity, and dynamics of the Venus thermosphere. Space Sci. Rev. **55**, 357-489.
81. Fox, J. L., and K. Y. Sung (2001). Solar activity variations of the Venus thermosphere/ionosphere. J. Geophys. Res. **106**, 21305-21335.
82. Friedson, A. J., A.-S. Wong, and Y. L. Yung (2002). Models for polar haze formation in Jupiter's stratosphere, Icarus **158**, 389-400.
83. Fulchignoni, M., Ferri, F., Angrilliet, F. et al., 2005. Titan's Physical Characteristics Measured by the Huygens Atmospheric Structure Instrument (HASI), Nature **438**, 785-791, doi:10.1038/nature04314, 2005.
84. Fuller-Rowell, T. J., D. Rees, S. Quegan, R. J. Moffett, M. V. Codrescu, and G. H. Millward (1996), A coupled thermosphere-ionosphere model (CTIM), in: *STEP Handbook of Ionospheric Models*, edited by Schunk, R. W., Utah State University, Logan, Utah, 217-238.

85. García Muñoz, A., J. C. McConnell, I. C. McDade, and S. M. L. Melo (2005). Airglow on Mars: Some model expectations for the OH Meinel bands and the O_2 IR atmospheric band, Icarus **176**, 75-95.
86. Geller, M. A. (1983), Dynamics of the Middle Atmosphere, Space Science Rev. **34**, 359-375.
87. Gierasch, P. (1975), Meridional circulation and the maintenance of the Venus atmospheric rotation. J. Atmos. Sci. **32**, 1038-1044.
88. Gierasch, P. J., R. M. Goody, R. E. Young, D. Crisp, C. Edwards, R. Kahn, D. Rider, A. Del Genio, R. Greeley, A. Hou, C. B. Leovy, D. McCleese, and M. Newman (1997), The general circulation of the Venus atmosphere: an assessment. In: S. W. Bougher, D. M. Hunten and R. J. Phillips, Editors, Venus II, University of Arizona Press, Tucson, 459-500.
89. Gladstone, G. R., M. Allen, and Y. L. Yung (1996). Hydrocarbon photochemistry in the upper atmosphere of Jupiter. Icarus **119**, 1-52.
90. González-Galindo, F., M. A. López-Valverde, M. Angelats i Coll, and F. Forget (2005), Extension of a Martian general circulation model to thermospheric altitudes: UV heating and photochemical models, J. Geophys. Res. **110**, doi:10.1029/2004JE002312.
91. Greathouse, T. K., J. H. Lacy, B. Bézard, J. I. Moses, C. A. Griffith, and M. J. Richter (2005). Meridional variations of temperature, C_2H_2 and C_2H_6 abundances in Saturn's stratosphere at southern summer solstice. Icarus **177**, 18-31.
92. Harris, M. J. (2000), A new coupled terrestrial mesosphere-thermosphere general circulation model: Studies of dynamic, energetic, and photochemical coupling in the middle and upper atmosphere, PhD Thesis, University of London, UK.
93. Harris, M. J., N. F. Arnold, and A. D. Aylward (2002), A study into the effect of the diurnal tide on the structure of the background mesosphere and thermosphere using the new coupled middle atmosphere and thermosphere (CMAT) general circulation model, Ann. Geophys. **20**, 225-235.
94. Hedin, A. E., E. L. Fleming, A. H. Manson, F. J. Schmidlin, S. K. Avery, R. R. Clark, S. J. Franke, G .J. A. Fraser, T. A. Tsuda, F. A. Vial, and R. A. Vincent (1996), Empirical wind model for the upper, middle and lower atmosphere, J. Atmos. Terr. Phys. **58**, 1421-1447.
95. Hesman, B. E., G. R. Davis, H. E. Matthews, and G. S. Orton (2007). The abundance profile of CO in Neptune's atmosphere. Icarus **186**, 342-353.
96. Hodges, R. R. (1999), Monte Carlo simulation of nonadiabatic expansion in cometary atmospheres - Halley, Icarus **83**, 410-423.
97. Hourdin, F., O. Talagrand, R. Sadourny, R. Courtin, D. Gautier, and C. P. Mc Kay (1995), Numerical simulation of the general circulation of the atmosphere of Titan, Icarus **117**, 358-374.
98. Howett, C. J. A., P. G. J. Irwin, N. A. Teanby, A. Simon-Miller, S. B. Calcutt, L. N. Fletcher, and R. de Kok (2007). Meridional variations in stratospheric acetylene and ethane in the Southern hemisphere of the saturnian atmosphere as determined from Cassini/CIRS measurements, Icarus **190**, 556-572.
99. Hubbard, W. B., et al. (1993), The occultation of 28 SGR by Titan, Astron. Astrophys. **269**, 541-563.
100. Hubbard, W. B., and 27 colleagues (1997), Structure of Saturn's mesosphere from the 28 Sgr occultations. Icarus **130**, 404-425.
101. Huebner, W. F., J. J. Keady, S. P. Lyon (1992), Astrophys. Space Sci. **195**, 1-294.
102. Huestis, D. L., S. W. Bougher, J. L. Fox, M. Galand, R. E. Johnson, J. I. Moses, and J. C. Pickering (2008), Cross Sections and Reaction Rates for Comparative Planetary Aeronomy, *this volume*.
103. Imanaka, H., and M. A. Smith (2007). Role of photoionization in the formation of complex organic molecules in Titan's upper atmosphere. Geophys. Res. Lett. **34**, L02204, doi:10.1029/2006GL028317.
104. Ingersoll, A. P., R. F. Beebe, B. J. Conrath, G. E. Hunt (1984), in: Saturn, T. Gehrels, M. S. Matthews, Eds., Univ. of Arizona Press, Tucson, 195-238.
105. Ip, W.-H. (1983), On photochemical heating of cometary comae - The cases of H_2O and CO-rich comets, Astrophys. J. **264**, 726-732.

106. Jessup, K. L., J. R. Spencer, G. E. Ballester, R. Howell, F. Roessler, M. Vigel, and R. .V. Yelle (2004). The atmospheric signature of Io's Prometheus plume and anti-jovian hemisphere: Evidence for a sublimation atmosphere. Icarus **169**, 197-215.
107. Jessup, K. L., J. Spencer, and R. V. Yelle (2007). Sulfur volcanism on Io. Icarus **192**, 24-40.
108. Kasprzak, W. T., A. E. Hedin, H. G. Mayr, and H. B. Niemann (1988), Wavelike perturbations observed in the neutral thermosphere of Venus, J. Geophys. Res. **93**, 11237-11245.
109. Keating, G.M. et al.(1998), The structure of the upper atmosphere of Mars: in situ accelerometer measurements from Mars Global Surveyor, Science **279**, 1672-1675.
110. Keller, H.A. Weaver (Univ. Arizona Press, Tucson, 2005), pp. 391-423
111. Krasnopolsky, V. A. (1986). Photochemistry of the Atmospheres of Mars and Venus. Springer-Verlag, Berlin.
112. Krasnopolsky, V. A. (1995). Uniqueness of a solution of a steady-state photochemical problem: Applications to Mars. J. Geophys. Res. **100**, 3263-3276.
113. Krasnopolsky, V. A. (2006a). Photochemistry in the martian atmosphere: Seasonal, latitudinal, and diurnal variations. Icarus **185**, 153-170.
114. Krasnopolsky, V. A. (2006b). Some problems related to the origin of methane on Mars. Icarus **180**, 359-367.
115. Krasnopolsky, V. A. (2006c). Chemical composition of Venus atmosphere and clouds: Some unsolved problems. Planet. Space Sci. **54**, 1352-1359.
116. Krasnopolsky, V. A. (2007). Chemical kinetic model for the lower atmosphere of Venus. Icarus **191**, 25-37.
117. Krasnopolsky, V. A., and D. P. Cruikshank (1995). Photochemistry of Triton's atmosphere and ionosphere. J. Geophys. Res. **100**, 21271-21286.
118. Krasnopolsky, V. A., and D. P. Cruikshank (1999). Photochemistry of Pluto's atmosphere and ionosphere near perihelion. J. Geophys. Res. **104**, 21979-21996.
119. Krasnopolsky, V. A., and V. A. Parshev (1983). Photochemistry of the Venus atmosphere. In Venus (D. M. Hunten, L. Colin, T. M. Donahue, V. I. Moroz, Eds.), pp. 431-458, University of Arizona Press, Tucson, AZ.
120. Krasnopolsky, V. A., and J. B. Pollack (1994). H_2O-H_2SO_4 system in Venus' clouds and OCS, CO, and H_2SO_4 profiles in Venus' troposphere. Icarus **109**, 58-78.
121. Krasnopolsky, V. A., J. P. Maillard, and T. C. Owen (2004). Detection of methane in the martian atmosphere: evidence for life? Icarus **172**, 537-547.
122. Krasnopolsky, V. A. (2007), Long-term spectroscopic observations of Mars using IRTF/CSHELL: Mapping of O_2 dayglow, CO, and search for CH_4, Icarus **190**, 93-102.
123. Kunde, V., and 41 co-authors (2004). Jupiter's atmospheric composition from the Cassini thermal infrared spectroscopy experiment. Science **305**, 1582-1587.
124. Lammer, H., et al. (2006). Loss of hydrogen and oxygen from the upper atmosphere of Venus. Planet. Space Sci. **54**, 1445-1456.
125. Lara, L. M., E. Lellouch, J. J. López-Moreno, and R. Rodrigo (1996). Vertical distribution of Titan's atmospheric neutral constituents, J. Geophys. Res. **113**, 2-26.
126. Lara, L. M., W.-H. Ip, and R. Rodrigo (1997). Photochemical models of Pluto's atmosphere. Icarus **130**, 16-35.
127. Laver, C., I. de Pater, H. Roe, and D. F. Strobel (2007). Temporal behavior of the SO 1.707 μm ro-vibronic emission band in Io's atmosphere. Icarus **189**, 401-408.
128. Lebonnois, S., D. Toublanc, F. Hourdin, and P. Rannou (2001). Seasonal variations of Titan's atmospheric composition. Icarus **152**, 384-406.
129. Lebonnois, S. (2005), Benzene and aerosol production in Titan and Jupiter's atmospheres: a sensitivity study. Planet. Space Sci. **53**, 486-497.
130. Lefèvre, F., S. Lebonnois, F. Montmessin, and F. Forget (2004). Threee-dimensional modeling of ozone on Mars. J. Geophys. Res. **109**, E07004, doi:10.1029/2004JE002268.
131. Lefèvre, F., J.-L. Bertaux, S. Perrier, S. Lebonnois, O. Korablev, A. Fedorova, F. Montmessin, and F. Forget (2007). The Martian ozone layer as seen by SPICAM/Mars-Express. Paper presented at the Seventh International Conference on Mars, 9-13 July 2007, Pasadena, California, 3137.

132. Lellouch, E., J. Rosenquist, J. J. Goldstein, S. W. Bougher, and G. Paubert (1991), First absolute wind measurements in the middle atmosphere of Mars, Astrophys. J. **383**, 401-406.
133. Lellouch, E., T. Clancy, D. Crisp, A. Kliore, D. Titov, and S. W. Bougher (1997), Monitoring of Mesospheric Structure and Dynamics. Venus II, CH. 3.1. University of Arizona Press, Tucson, 295-324.
134. Lellouch, E., P. N. Romani, and J. Rosenqvist (1994). The vertical distribution and origin of HCN in Neptune's atmosphere. Icarus **108**, 112-136.
135. Lellouch, E. B. Bézard, J. I. Moses, G. R. Davis, P. Drossart, H. Feuchtgruber, E. A. Bergin, R. Moreno, and T. Encrenaz (2002). The origin of water vapor and carbon dioxide in Jupiter's stratosphere. Icarus **159**, 112-131.
136. Lellouch, E., G. Paubert, J. I. Moses, N. M. Schneider, and D. F. Strobel (2003). Volcanically emitted sodium chloride as a source for Io's neutral clouds and plasma torus, Nature **421**, 45-47.
137. Lellouch, E., R. Moreno, and G. Paubert (2005). A dual origin for Neptune's carbon monoxide, Astron. Astrophys. **430**, L37-L40.
138. Lellouch, E., B. Bézard, D. F. Strobel, G. L. Bjoraker, F. M. Flasar, and P. N. Romani (2006). On the HCN and CO_2 abundance and distribution in Jupiter's stratosphere. Icarus **184**, 478-497.
139. Liang, M.-C., R.-L. Shia, A. Y.-T. Lee, M. Allen, A. J. Friedson, and Y. L. Yung (2005). Meridional transport in the stratosphere of Jupiter. Astrophys. J. **635**, L177-L180.
140. Lindal, G. F., The atmosphere of Neptune: An analysis of the radio occultation data acquired with Voyager 2, Astron. J. **103**, 967-972, 1992.
141. Lindzen, R. S. (1981), Turbulence and stress owing to gravity wave and tidal breakdown, J. Geophys. Res. **86**, 9707-9714.
142. Lis, D., D. Bockelée-Morvan, N. Biver, et al. (2008), Hydrogen isocyanide in comet 73P/Schwassmann-Wachmann (fragment B), Astrophys. J. **675**, 931-936.
143. Luz, D., F. Hourdin, P. Rannou, and S. Lebonnois (2003). Latitudinal transport by barotropic waves in Titan's stratosphere. II. Results from a coupled dynamics-microphysics-photochemistry GCM. Icarus **166**, 343-358.
144. Lyons, J. R., C. Manning, and F. Nimmo (2005). Formation of methane on Mars by fluid-rock interaction in the crust. Geophys. Res. Lett. **32**, L13201, doi:10.1029/ 2004GL022161.
145. Majeed, T., J. H. Waite, Jr., S. W. Bougher, and G. R. Gladstone (2005), Processes of equatorial thermal structure at Jupiter: An analysis of the Galileo temperature profile with a three-dimensional model, J. Geophys. Res. **110**, E12007, doi:10.1029/2004JE002351.
146. Mayr, H. G., I. Harris, W. T. Kasprzak, M. Dube, and F. Varosi (1988), Gravity waves in the upper atmosphere of Venus, J. Geophys. Res. **93**, 11247-11262.
147. Max, M. D., and S. M. Clifford (2000). The state, potential distribution, and biological implications of methane in the Martian crust. J. Geophys. Res. **105**, 4165-4172.
148. McElroy, M. B., and T. M. Donahue (1972). Stability of the Martian atmosphere. J. Atmos. Sci. **28**, 879-884.
149. Medvedev, A. S., and G. P. Klaassen (2000), Parameterization of gravity wave momentum deposition based on nonlinear wave interactions: basic formulation and sensitivity tests, J. Atmos. Sol.-Terr. Phys. **62**, 1015-1033.
150. Meyer, C. K. (1999), Gravity wave interactions with mesospheric planetary waves: A mechanism for penetration into the thermosphere-ionosphere system, J. Geophys. Res. **104**, 28181-28196.
151. Mills, F. P. (1998). I. Observations and photochemical modeling of the Venus middle atmosphere. II. Thermal infrared spectroscopy of Europa and Callisto. Ph.D. Thesis. California Institute of Technology, Pasadena, CA.
152. Mills, F. P., and M. Allen (2007). A review of selected issues concerning the chemistry in Venus' middle atmosphere. Planet. Space Sci. **55**, 1729-1740.
153. Mills, F. P., M. Sundaram, T. G. Slanger, M. Allen, and Y. L. Yung (2006). Oxygen chemistry in the Venus middle atmosphere. In Advances in Geosciences Volume 3: Planetary Science (W.-H. Ip and A. Bhardwaj, Eds.), 109-117, World Scientific Publishing Co., Singapore.

154. Molina-Cuberos, G. J., K. Schwingenschuh, J. J. López-Moreno, R. Rodrigo, L. M. Lara, and V. Anicich (2002). Nitriles produced by ion chemistry in the lower ionosphere of Titan. J. Geophys. Res. **107**, 5099, doi:10.1029/ 2000JE001480.
155. Moreau, D., L. W. Esposito, and G. Brasseur (1991). The chemical composition of the dust-free Martian atmosphere: Preliminary results of a two-dimensional model. J. Geophys. Res. **96**, 7933-7945.
156. Moses, J. I., and T. K. Greathouse (2005), Latitudinal and seasonal models of stratospheric photochemistry on Saturn: Comparison with infrared data from ITRF/TEXES. J. Geophys. Res. **110**, E09007, doi:10.1029/ 2005JE002450.
157. Moses, J. I., B. Bézard, E. Lellouch, G. R. Gladstone, H. Feuchtgruber, and M. Allen (2000a). Photochemistry of Saturn's atmosphere. I. Hydrocarbon chemistry and comparisons with ISO observations. Icarus **143**, 244-298.
158. Moses, J. I., E. Lellouch, B. Bézard, G. R. Gladstone, H. Feuchtgruber, and M. Allen (2000b). Photochemistry of Saturn's atmosphere. II. Effects of an influx of external material. Icarus **145**, 166-202.
159. Moses, J. I., M. Y. Zolotov, and B. Fegley, Jr. (2002a). Photochemistry of a volcanically driven atmosphere on Io: Sulfur and oxygen species from a Pele-type eruption. Icarus **156**, 76-106.
160. Moses, J. I., M. Y. Zolotov, and B. Fegley, Jr. (2002b). Alkali and chlorine photochemistry in a volcanically driven atmosphere on Io. Icarus **156**, 107-135.
161. Moses, J. I., T. Fouchet, R. V. Yelle, A. J. Friedson, G. S. Orton, B. Bézard, P. Drossart, G. R. Gladstone, T. Kostiuk, and T. A. Livengood (2004). The stratosphere of Jupiter. In Jupiter: Planet, Satellites and Magnetosphere (F. Bagenal, W. McKinnon, and T. Dowling, Eds.), 129-157, Cambridge Univ. Press, New York.
162. Moses, J. I., T. Fouchet, B. Bézard, G. R. Gladstone, E. Lellouch, and H. Feuchtgruber (2005). Photochemistry and diffusion in Jupiter's stratosphere: Constraints from ISO observations and comparisons with other giant planets. J. Geophys. Res. **110**, E08001, doi:10.1029/ 2005JE002411.
163. Moses, J. I., M.-C. Liang, Y. L. Yung, and R.-L. Shia (2007). Meridional distribution of hydrocarbons on Saturn: Implications for stratospheric transport. Paper presented at the Planetary Atmospheres Workshop, 6-7 Nov. 2007, Greenbelt, MD, 85-86.
164. Moudden, Y. (2007). Simulated seasonal variations of hydrogen peroxide in the atmosphere of Mars. Planet. Space Sci. **55**, 2137-2143.
165. Moudden, Y., and J. C. McConnell (2007). Three-dimensional on-line chemical modeling in a Mars general circulation model. Icarus **188**, 18-34.
166. Mueller-Wodarg, I. C. F., R. V. Yelle, M. Mendillo, and A. D. Aylward (2003), On the global distribution of neutral gases in Titan's upper atmosphere and its effect on the thermal structure, J. Geophys. Res., **108**, doi:10.1029/2003JA010054.
167. Mueller-Wodarg, I. C. F., M. Mendillo, R. V. Yelle, and A. D. Aylward (2006a), A global circulation model of Saturn's thermosphere, Icarus, **180**, 147-160.
168. Mueller-Wodarg, I C. F., R. V. Yelle, N. Borggren, and J. H. Waite (2006b), Waves and horizontal structures in Titans thermosphere, J. Geophys. Res., **111**, A12315, doi:10.1029/2006JA011961.
169. Mueller-Wodarg, I C. F., R. V. Yelle, J. Cui., and J. H. Waite (2008), Horizontal structures and dynamics of Titan's thermosphere, J. Geophys. Res., in press.
170. Mumma, M. L., M. A. DiSanti, N. Dello Russo, et al. (2003), Remote infrared observations of parent volatiles in comets: A window on the early solar system, Adv. Space Res. **31**, 2563-2575.
171. Nair, H., M. Allen, A. D. Anbar, Y. L. Yung, and R. T. Clancy (1994). A photochemical model of the Martian atmosphere, Icarus **111**, 124-150.
172. Nixon, C. A., R. K. Achterberg, B. J. Conrath, P. G. J. Irwin, N. A. Teanby, T. Fouchet, P. D. Parrish, P. N. Romani, M. Abbas, A. LeClair, D. Strobel, A. A. Simon-Miller, D. J. Jennings, F. M. Flasar, and V. G. Kunde (2007). Meridional variations of C_2H_2 and C_2H_6 in Jupiter's atmosphere from Cassini CIRS infrared spectra, Icarus **188**, 47-71.

173. Orton, G. et al. (1996), Earth-based observations of the Galileo probe entry site. Science **272**, 839-840.
174. Owen, T. et al. (1977), The compostion of the atmosphere at the surface of Mars, J. Geophys. Res., **82**, 4635-4639.
175. Owen, T., A. Bar-Nun, and I. Kleinfeld (1992), Possible cometary origin of heavy noble gases in the atmospheres of Venus, Earth, and Mars, Nature, **358**, 43-46, doi: 10.1038/358043a0
176. Owen, T. (2007), Planetary atmospheres, Space Sci. Rev., **130**, 97-104, DOI 10.1007/s11214-007-9233-z.
177. Oze, C., and M. Sharma (2005). Have olivine, will gas: Serpentization and the abiogenic production of methane on Mars. Geophys. Res. Lett. **32**, L10203, doi:10.1029/ 2005GL022691.
178. Parkinson, T. M., and D. M. Hunten (1972). Spectroscopy and aeronomy of O_2 on Mars. J. Atmos. Sci. **29**, 1380-1390.
179. Pernice, H., P. Garcia, H. Willner, J. S. Francisco, F. P. Mills, M. Allen, and Y. L. Yung (2004). Laboratory evidence for a key intermediate in the Venus atmosphere: Peroxychloroformyl radical. Proc. Natl. Acad. Sci. **101**, 14007-14010.
180. Prangé, R., T. Fouchet, R. Courtin, J. E. P. Connerney, and J. C. McConnell (2006). Latitudinal variation of Saturn photochemistry deduced from spatially-resolved ultraviolet spectra. Icarus **180**, 379-392.
181. Rego, D., N. Achilleos, T. Stallard, S. Miller, R. Prangé, M. K. Dougherty, and R. Joseph (1999), Supersonic winds in Jupiter's aurorae, Nature **399**, 121-124, doi: 10.1038/20121.
182. Rishbeth, H, and I. C. F. Mueller-Wodarg (1999), Vertical circulation and thermospheric composition: a modelling study, Ann.Geophysicae, **17**, 794-805.
183. Roble, R. G. (1996), On Solar Induced Variability in the Earth's Upper Atmosphere and Ionosphere, Astron. Soc. of the Pacific, Eds. K. S. Balasubramaniam, S. L. Keil, and R. N. Smartt, 609.
184. Roble, R. G., R. E. Dickinson, E. C. Ridley, B. A. Emery, P. B. Hays, T. L. Killeen, and N. W. Spencer (1983), The high latitude circulation and temperature structure of the thermosphere near solstice, Planet. Sp. Science **31**, 1479-1499, doi:10.1016/0032-0633(83)90021-1.
185. Roble, R. G., E. C. Ridley, A. D. Richmond, and D. E. Dickinson (1988), A coupled Thermosphere-Ionosphere General Circulation Model, Geophys. Res. Lett. **15**, 1325-1328.
186. Roble, R. G., and E. C. Ridley (1994), A thermosphere-ionosphere-mesosphere-electrodynamics general circulation model (TIME-GCM): Equinox solar cycle minimum simulations (30500 km), Geophys. Res. Lett. **21**, 417-420.
187. Rogers, S. D., S.B. Charnley, W.F. Huebner, D.C. Boice (2005), Physical processes and chemical reactions in cometary comae, in: *Comets II*, ed. by M. C. Festou, H. U. Keller, H. A. Weaver, Univ. Arizona Press, Tucson, 505-522.
188. Romani, P. N. (1996). Recent rate constant and product measurements of the reactions C_2H_3 + H_2 and C_2H_3 + H — Importance for photochemical modeling of hydrocarbons on Jupiter. Icarus **122**, 233-241.
189. Romani, P. N., and S. K. Atreya (1988). Methane photochemistry and haze production on Neptune, Icarus **74**, 424-445.
190. Romani, P. N., J. Bishop, B. Bézard, and S. Atreya (1993). Methane photochemistry on Neptune: Ethane and acetylene mixing ratios and haze production, Icarus **106**, 442-463.
191. Sánchez-Lavega, A., S. Pérez-Hoyos, J. F. Rojas, R. Hues, and R. G. French (2003), Nature **423**, 623.
192. Saur, J., and D. F. Strobel (2004). Relative contributions of sublimation and volcanoes to Io's atmosphere from its plasma interaction during solar eclipse, Icarus **171**, 411-420.
193. Schaefer, L., and B. Fegley (2004). A thermodynamic model of high temperature lava vaporization on Io, Icarus **169**, 216-241.
194. Schaefer, L., and B. Fegley (2005a). Predicted abundances of carbon compounds in volcanic gases on Io. Astrophys. J. **618**, 1079-1085.
195. Schaefer, L., and B. Fegley (2005b). Alkali and halogen chemistry in volcanic gases on Io. Icarus **173**, 454-468.
196. Schaefer, L., and B. Fegley (2005c). Silicon tetrafluoride on Io. Icarus **179**, 252-258.

197. Schoeberl, M. R., and D. F. Strobel (1978), The zonally averaged circulation of the middle atmosphere, J. Atm. Sci. **35**, 577-591.
198. Schofield, J. T., and F. W. Taylor (1983), Measurements of the mean solar-fixed temperature and cloud structure in the middle atmosphere of Venus, Q. J. R. Meteorol. Soc. **109**, 57-80.
199. Schubert, G. (1983), General circulation and dynamical state of the Venus atmosphere. In: Hunten, D. M., et al. (Eds.), Venus. Univ. of Arizona Press, Tucson, 681-765.
200. Schubert, G., et al. (2007), "Venus Atmosphere Dynamics: A Continuing Enigma", in: Exploring Venus as a Terrestrial Planet, Geophysical Monograph 176, American Geophysical Union, 101-120.
201. Seiff, A., Models of Venuss atmospheric structure, in Venus, edited by D. M. Hunten, L. Colin, and V. I. Moroz, Univ. Arizona Press, Tucson, 1045-1048, 1983.
202. Seiff, A., et a. (1997), Thermal structure of Jupiter's upper atmosphere derived from the Galileo probe, Science, **276**, 102-104.
203. Seinfeld, J. H., and S. N. Pandis (2006). Atmospheric Chemistry and Physics: From Air Pollution to Climate Change. Wiley-Interscience, Hoboken, New Jersey.
204. Senay, M. C., D. Jewitt (1994), Coma formation driven by carbon-monoxide release from comet Schwassmann-Wachmann 1, Nature **371**, 229-231.
205. Sicardy, B., et al. (2006), The two Titan stellar occultations of 14 November 2003, J. Geophys. Res. **111**, E11S91, doi:10.1029/2005JE002624.
206. Slanger, T., D. L. Huestis, P. C. Cosby, N. J. Chanover, and T. A. Bida (2006). The Venus nightglow: Ground-based observations and chemical mechanisms, Icarus **182**, 1-9.
207. Smith, C. G. A., A. D. Aylward, G. H. Millward, S. Miller, and L. E. Moore (2007), An unexpected cooling effect in Saturn's upper atmosphere, Nature **445**, 399-401, doi:10.1038/nature05518.
208. Smyth, W. H., and M. C. Wong (2004). Impact of electron chemistry on the structure and composition of Io's atmosphere. Icarus **171**, 171-182.
209. Spencer, J. R., K. L. Jessup, M. A. McGrath, G. E. Ballester, and R. Yelle 2000. Discovery of gaseous S_2 in Io's Pele plume. Science **288**, 1208-1210.
210. Stallard, T., S. Miller, G. Millward, and R. D. Joseph (2001), On the dynamics of the jovian ionosphere and thermosphere. I. The measurement of ion winds, Icarus **154**, 475-491.
211. T. Stallard, S. MillerH. Melin, M. LystrupM. K. Dougherty, and N. Achilleos (2007), Saturn's auroral/polar H_3^+ infrared emission - I. General morphology and ion velocity structure, Icarus **189**, 1-13, doi:10.1016/j.icarus.2006.12.027.
212. Stevens, M. H., D. F. Strobel, and F. Herbert, An analysis of the Voyager 2 ultraviolet spectrometer occultation data at Uranus: Inferring heat sources and model atmospheres, Icarus **100**, 45-63, 1993.
213. Strobel, D. F. (2005). Photochemistry in outer solar system atmospheres. Space Sci. Rev. **116**, 155-170.
214. Strobel, D. F., Titan's hydrodynamically escaping atmosphere, Icarus **193**, 588-594, doi:10.1016/j.icarus.2007.08.014, 2008a.
215. Strobel, D. F., N_2 Escape rates from Pluto's atmosphere, Icarus **193**, 612-619, doi:10.1016/j.icarus.2007.08.021, 2008b.
216. Strobel, D. F., and M. E. Summers (1995). Triton's upper atmosphere and ionosphere. In Neptune and Triton (D. P. Cruikshank, Ed.), 1107-1148, Univ. Arizona Press, Tucson.
217. Strobel, D. F., and B. C. Wolven 2001. The atmosphere of Io: Abundances and sources of sulfur dioxide and atomic hydrogen, Astrophys. Space Sci. **277**, 271-287.
218. Summers, M. E., and D. F. Strobel (1989). Photochemistry of the atmosphere of Uranus, Astrophys. J. **346**, 495-508.
219. Summers, M. E., and D. F. Strobel (1996). Photochemistry and vertical transport in Io's atmosphere and ionosphere, Icarus **120**, 290-316.
220. Sunshine, J. M. , M. F. A'Hearn, O. Groussin, et al. (2007), Exposed water ice deposits on the surface of comet 9P/Tempel 1, Science **311**, 1453-1455.
221. Strobel, D. F., X. Zhu, and M. E. Summers, On the Vertical Thermal Structure of Pluto's Atmosphere, Icarus **120**, 266-289, 1996.

222. Summers, M. E., D. F. Strobel, and G. R. Gladstone (1997). Chemical models of Pluto's atmosphere. In Pluto (S. A. Stern and D. J. Tholen (Eds.), pp. 391-434, Univ. Arizona Press, Tucson.
223. Toublanc, D., J. P. Parisot, J. Brillet, D. Gautier, F. Raulin, and C. P. McKay (1995). Photochemical modeling of Titan's atmosphere. Icarus **113**, 2-26.
224. Tseng, W.-L., D. Bockelée-Morvan, J. Crovisier, P. Colom, W.-H. Ip (2007), Cometary water expansion velocity from OH line shapes, Astron. Astrophys. **467**, 729-735.
225. Villanueva, G. L., B. P. Bonev, M. J. Mumma, et al. (2006), The volatile composition of the split ecliptic comet 73P/Schwassmann-Wachmann 3: A comparison of fragments C and B, Astrophys. J. **650**, L87-L90.
226. Vuitton, V., R. V. Yelle, and V. G. Anicich (2006). The nitrogen chemistry of Titan's upper atmosphere revealed. Astrophys. J. **647**, L175-L178.
227. Vuitton, V., R. V. Yelle, and M. J. McEwan (2007). Ion chemistry and N-containing molecules in Titan's upper atmosphere. Icarus **191**, 722-742.
228. Waite, J. H., et al. (2005). Ion Neutral Mass Spectrometer results from the first flyby of Titan. Science, **308**, 982-986.
229. Waite, J. H., D. T. Young, T. E. Cravens, A. J. Coates, F. J. Crary, B. Magee, and J. Westlake (2007). The process of tholin formation in Titan's upper atmosphere. Science, **316**, 870-875.
230. Wayne, R. P. (2000). Chemistry of Atmospheres. Oxford University Press, Oxford.
231. Wilson, E. H., and S. K. Atreya (2004). Current state of modeling the photochemistry of Titan's mutually dependent atmosphere and ionosphere. J. Geophys. Res. **109**, E06002, doi:10.1029/ 2003JE002181.
232. Wilson, E. H., S. K. Atreya, and A. Coustenis (2003). Mechanisms for the formation of benzene in the atmosphere of Titan. J. Geophys. Res. **108**, 5014, doi:10.1029/ 2002JE001896.
233. Winick, J. R., and A. I. Stewart (1980). Photochemistry of SO_2 in Venus' upper cloud layers. J. Geophys. Res. **85**, 7849-7860.
234. Witasse, O., T. Cravens, M. Mendillo, J. Moses, A. Kliore, A. F. Nagy, and T. Breus (2008), Ionospheres, *this volume*.
235. Withers, P., Bougher, S. W., Keating, G. M. (2003), The effects of topographically-controlled thermal tides in the martian upper atmosphere as seen by the MGS accelerometer, Icarus **164**, 14-32.
236. Wong, M. C., and R. E. Johnson (1996). A three-dimensional azimuthally symmetric model atmosphere for Io. 1. Photochemistry and the accumulation of a nightside atmosphere. J. Geophys. Res. **101**, 23243-23254.
237. Wong, M. C., and W. H. Smyth (2000). Model calculations for Io's atmosphere at eastern and western elongations. Icarus **146**, 60-74.
238. Wong, A.-S., A. Y. T. Lee, Y. L. Yung, and J. M. Ajello (2000). Jupiter: Aerosol chemistry in the polar atmosphere. Astrophys. J. **534**, L215-L217.
239. Wong, A.-S., C. G. Morgan, and Y. L. Yung (2002). Evolution of CO on Titan. Icarus **155**, 382-392.
240. Wong, A.-S., Y. L. Yung, and A. J. Friedson (2003). Benzene and haze formation in the polar atmosphere of Jupiter. Geophys. Res. Lett. **30**, 1447, doi:10.1029/ 2002GL016661.
241. Wong, A. S., S. K. Atreya, V. Formisano, T. Encrenaz, and N. I. Ignatiev (2004). Adv. Space Res. **33**, 2236-2239.
242. Yamazaki, Y. H., D. R. Skeet, and P. L. Read (2004), A new general circulation model of Jupiter's atmosphere based on the UKMO Unified Model: Three-dimensional evolution of isolated vortices and zonal jets in mid-latitudes, Planet. Sp. Sci. **52**, 423-445, doi:10.1016/j.pss.2003.06.006.
243. Yelle, R. V. (1991), Non-LTE models of Titan's upper atmosphere, Astrophys. J., **383**, 380-400.
244. Yelle, R. V., and J. I. Lunine (1989), Evidence for a molecule heavier than methane in the atmosphere of Pluto, Nature **339**, 288-290.
245. Yelle, R. V., L. R. Doose, M. G. Tomasko, and D. F. Strobel, Analysis of Raman Scattered Ly-Alpha Emissions from the Atmosphere of Uranus (1987), Geophys. Res. Lett. **14**, 483.

246. Yelle, R. V., C. A. Griffith, and L. A. Young (2001). Structure of the Jovian stratosphere at the Galileo probe entry site, Icarus **152**, 331-346.
247. Yelle, R. V., and S. Miller (2004), Jupiter's Thermosphere and Ionosphere, in: *Jupiter, The Planet, Satellites and Magnetosphere*, F. Bagenal, T. E. Dowling and W. B. McKinnon, Editors, Cambridge University Press, Cambridge.
248. Yelle, R. V., N. Borggren, V. de la Haye, W. T. Kasprzak, H. B. Niemann, I. C. F. Mueller-Wodarg, and J. H. Waite Jr. (2006), The vertical structure of Titan's upper atmosphere from Cassini Ion Neutral Mass Spectrometer measurements, Icarus, **182**, 567-576.
249. Yelle, R. V., J. Cui, and I. C. F. Mueller-Wodarg (2008), Eddy Diffusion and Methane Escape from Titan's Atmosphere, J. Geophys. Res., *in press*.
250. Yung, Y. L., and W. B. DeMore (1982). Yung, Y. L., and W. B. DeMore (1982). Photochemistry of the stratosphere of Venus: Implications for atmospheric evolution. Icarus **51**, 199-247.
251. Yung, Y. L., and W. B. DeMore (1999). Photochemistry of Planetary Atmospheres. Oxford University Press, New York.
252. Yung, Y. L., D. F. Strobel, T. Y. Kong, and M. B. McElroy (1977). Photochemistry of nitrogen in the Martian atmosphere, Icarus **30**, 26-41.
253. Yung, Y. L., M. Allen, and J. P. Pinto (1984). Photochemistry of the atmosphere of Titan: Comparison between model and observations. Astrophys. J. Suppl. Ser. **55**, 465-506.
254. Zhang, J., D. B. Goldstein, P. L. Varghese, N. E. Gimelshein, S. F. Gimelshein, and D. A. Levin (2003). Simulation of gas dynamics and radiation in volcanic plumes on Io. Icarus **163**, 182-197.
255. Zhang, J., D. B. Goldstein, P. L. Varghese, L. Trafton, C. Moore, and K. Miki (2004). Numerical modeling of ionian volcanis plumes with entrained particulates. Icarus **172**, 479-502.
256. Zhou, Q. H., M. P. Sulzer, C. A. Tepley, C. G. Fesen, R. G. Roble, and M. C. Kelley (1997), Neutral winds and temperature in the tropical mesosphere and lower thermosphere during January 1993: Observation and comparison with TIME-GCM results, J. Geophys. Res., **102**, 11,507-11,519.
257. Zhu, X., and J.-H. Yee (2007). Wave-photochemistry coupling and its effect on water vapor, ozone and airglow variations in the atmosphere of Mars, Icarus **189**, 136-150.
258. Zolotov, M. Yu., and B. Fegley, Jr. 1998a. Volcanic origin of disulfur monoxide (S_2O) on Io, Icarus **133**, 293-297.
259. Zolotov, M. Yu., and B. Fegley, Jr. 1998b. Volcanic production of sulfur monoxide (SO) on Io, Icarus **132**, 431-434.
260. Zolotov, M. Yu., and B. Fegley, Jr. 1999. Oxidation state of volcanic gases and the interior of Io, Icarus **141**, 40-52.
261. Zolotov, M. Yu., and B. Fegley, Jr. 2000. Eruption conditions of Pele volcano on Io inferred from chemistry of its volcanic plume, Geophys. Res. Lett. **27**, 2789-2792.